pH dependent direct sulfhydrylation pathway is required for pathogenesis of *Mycobacterium tuberculosis*

1 Vaibhav Kumar Nain[1,2], Vishawjeet Barik[1,2#], Manitosh Pandey[1#], Mohit Pareek[3], Taruna Sharma[1,2],
2 Rahul Pal[1], Shaifali Tyagi[1], Manish Bajpai[4], Prabhanjan Dwivedi[5], Bhishma Narayan Panda[5],
3 Yashwant Kumar[4], Shailendra Asthana[3] and Amit Kumar Pandey[1,5*]

4 [1]Mycobacterial Pathogenesis Laboratory, Centre for Tuberculosis Research, BRIC-Translational
5 Health Science and Technology Institute, Haryana, India
6 [2]Special Centre for Molecular Medicine, Jawaharlal Nehru University, New Delhi, India
7 [3]Computational Biophysics and CADD Group, Computational and Mathematical Biology Centre,
8 BRIC-Translational Health Science and Technology Institute, Haryana, India
9 [4]Biomarker Discovery Laboratory, Non-Communicable Diseases Centre, BRIC-Translational Health
10 Science and Technology Institute, Haryana, India
11 [5]Experimental Animal Facility, BRIC-Translational Health Science and Technology Institute,
12 Haryana, India
13 [#] Contributed equally to this work
14 *** Correspondence:** Amit Kumar Pandey, amitpandey@thsti.res.in

15

16 **Abstract**

17 Methionine is essential for the survival of *Mycobacterium tuberculosis* (*M. tuberculosis*) inside the
18 host. Inhibiting the transsulfuration pathway fails to exhibit methionine auxotrophy suggesting the
19 presence of an alternate methionine biosynthesis pathway in *M. tuberculosis*. Orthologues of $MetZ_{TB}$
20 in other bacterial species are known to regulate a redundant single step methionine biosynthesis

pathway known as *direct sulfhydrylation.* Genetic disruption of the *metZ*-mediated direct sulfhydrylation pathway impaired the ability of *M. tuberculosis* to survive inside macrophages. Further, we demonstrated that direct sulfhydrylation pathway is indispensable for the survival at low pH. Using *in-silico* molecular docking and MD simulations studies we showed that the active site of MetZ binds substrate O-succinyl homoserine (OSH) more tightly at acidic rather than neutral pH. Intriguingly, despite higher intracellular ATP levels, a relative decrease in the frequency of generation of Bedaquiline (BDQ)-induced persisters in *ΔmetZ* suggests a role of direct sulfhydrylation pathway in modulating BDQ sensitivity in *M. tuberculosis*. Finally, using an animal model, we demonstrated that absence of *metZ* impeded the ability of *M. tuberculosis* to grow inside the host. Our findings suggest that administering inhibitors of *metZ* as an adjunct can be explored as a strategy to potentiate BDQ as a novel anti-TB regimen.

Keywords: tuberculosis, methionine biosynthesis, acidic pH, drug tolerance, transsulfuration, direct sulfhydrylation.

Introduction

Tuberculosis is one of the ancient diseases that remains a global threat to this day posing a great socio-economic threat to global public healthcare. As of 2023, *Mycobacterium tuberculosis* (*M. tuberculosis*) caused 1.8 million deaths making it the highest killing disease [1]. A gradual increase in the frequency of emergence of drug resistance cases has further complicated the therapeutic landscape against tuberculosis. A majority of drugs approved for treating tuberculosis are focused on targeting essential genes critical for survival of *M. tuberculosis* such as transcription, lipid biosynthesis, ATP synthesis, protein synthesis, etc. Targeting essential amino acid biosynthesis pathways (such as tryptophan,

44 arginine, proline, histidine, aspartate, etc.) as a therapeutic strategy against tuberculosis has
45 demonstrated immense potential and might lead to molecules with the potential to become a future
46 drug [2].
47 Methionine is required for maintenance of various biochemical processes to sustain life and regulation
48 of methionine biosynthesis becomes more consequential as, *N-formyl*-L-methionine (*f*Met), is known
49 to initiate translation in prokaryotes [3] and protein degradation in eukaryotes [4]. Further, it is required
50 for biosynthesis of other key metabolites – cysteine, biotin, SAM (S-adenosylmethionine), etc.
51 involved in several physiological and regulatory mechanisms. Historically, targeting the methionine
52 biosynthesis pathway as a strategy to identify new drugs against tuberculosis has been extensively
53 explored in various studies [5-9]. The transsulfuration pathway consisting of a sequence of reactions,
54 enzymes and intermediates involved in methionine biosynthesis are largely conserved across various
55 microbial species and has been extensively reviewed [10]. However, other than *metA/X, metH* genes
56 which have been reported to be essential for the growth of *M. tuberculosis in-vitro* as well as *in-vivo*
57 [5, 7, 11], some of the genes belonging to this pathway are dispensable for growth of *M. tuberculosis*
58 and hence, are either redundant or are conditionally essential [12-14]. There are reports which suggest
59 that there exists another biochemical reaction wherein O-succinyl homoserine (OSH) is directly
60 converted into homocysteine [13, 15]. Interestingly, biological H_2S, instead of cysteine is used as S-
61 donor in this reaction driven by an enzyme O-succinyl homoserine sulfhydrylase (OSHS) that bypasses
62 the two-step conversion of OSH to homocysteine, via cystathionine as intermediate step. This direct
63 conversion of OSH into homocysteine is called direct sulfhydrylation. Still uncharacterized in *M.*
64 *tuberculosis,* direct sulfhydrylation pathway is functional in several microbial species such as
65 *Pseudomonas aeruginosa [16], Leptospira [17]* and *Corynebacterium glutamicum [10, 18]. M.*
66 *tuberculosis* harbors a putative OSHS encoded by *metZ* (*Rv0391*) which is yet to be studied for its role
67 in direct sulfhydrylation pathway.

68 In this study, we have used genetics and computational biology-based tools to address the necessity of
69 *M. tuberculosis* to harbor redundant methionine biosynthesis pathways. We find that *metZ* null mutant
70 in *M. tuberculosis* is dispensable for growth at neutral pH, however, it is required for survival of the
71 bacterium at acidic pH, *ex-vivo* and *in-vivo*. It was also observed using computational approach that
72 MetZ protein, although stable at both acidic and neutral pH, the active site of the protein held the
73 substrate more stably at acidic pH than at neutral pH. Finally, using CRISPRi we prove that *metZ* in
74 *M. tuberculosis* is independent of transsulfuration pathway and involved in methionine biosynthesis as
75 corroborated by methionine levels in the mutant strain lacking both transsulfuration as well as direct
76 sulfhydrylation. In sum, we report that *metZ* is required for methionine biosynthesis via direct
77 sulfhydrylation pathway at acidic pH when transsulfuration fails to keep up with the cellular
78 requirements.

79 **Results**

80 **MetZ is dispensable for the *in-vitro* growth of *M. tuberculosis* and possibly involved in direct**
81 **sulfhydrylation pathway for methionine biosynthesis**

82 While *metZ* has been reported to be essential for growth in cholesterol [19], we hypothesize that the
83 *Rv0391 (metZ)* gene encodes a putative O-succinylhomoserine sulfhydrylase (OSHS) that is
84 responsible for direct sulfhydrylation (Fig. 1A). We performed a bioinformatics-based analysis using
85 the protein sequence of $MetZ_{TB}$ and found that the putative sequence belonged to the cluster of
86 orthologues group ENOG502GJ5S which is composed of 1097 protein sequences orthologous to
87 $MetZ_{TB}$ across 644 bacterial species. This cluster of proteins comprises various enzymes involved in
88 cellular amino acid metabolism namely, cysteine, methionine, homocysteine, serine and aspartate
89 family of amino acids. Interestingly, all these proteins have common PLP (pyridoxal-5-phosphate) –
90 binding domain which is essentially a modified lysine residue that covalently binds the co-factor, hence
91 also categorized as PLP-binding superfamily of proteins. (Fig. 1B and S1A). Further, to elucidate the

92 role of *metZ* in *M. tuberculosis*, a deletion mutant in the genetic background of H37Rv was generated
93 by genetic recombineering as described previously [20]. Briefly, a hygromycin resistance cassette was
94 inserted into the ORF encoding *metZ* (*Rv0391*) with the help of allelic exchange substrate (AES)
95 consisting of 1kb regions of homology upstream and downstream to the target locus. The recombinants
96 were screened for hygromycin resistance and the cassette was subsequently excised out thereby
97 generating unmarked mutant (Fig. 1C). The loss of the genetic sequence between 470034-471188 bases
98 was confirmed by gene-specific PCR (Fig. S2A), DNA sequencing of the locus (Fig. S2B) and at the
99 transcript level by RT-qPCR (Fig 1D). In order to check the essentiality of the *metZ* in growth in
100 cholesterol, we compared the growth of H37Rv, *ΔmetZ* and the complemented strains in different
101 media containing glycerol (0.1%), cholesterol (150µM), propionate (10mM) as the sole carbon source.
102 As a control, we used the *M. tuberculosis* strain lacking the *prpR* gene (*ΔprpR)* which is known to be
103 essential for growth in cholesterol [21]. While, as expected, *ΔprpR* failed to grow on cholesterol and
104 propionate*,* the growth of all the three strains were comparable irrespective to the carbon source (Figs.
105 1E, 1F and S3B). These findings indicate *metZ* does not contribute to the central carbon metabolism
106 and is dispensable for *in-vitro* growth in *M. tuberculosis* on cholesterol and/ or propionate.

107 ***metZ* deletion renders *M. tuberculosis* sensitive to physiological stressors and lead to reduced *ex-***
108 ***vivo* fitness**

109 In order to replicate and grow inside the host, intracellular pathogens have evolved mechanisms to
110 neutralize the host-induced physiological stressors which include redox, cell membrane and pH stress.
111 These *in-vitro* induced stress conditions mimic *in-vivo* growth conditions, wherein bacterial cells were
112 subjected to different stress inducing reagents and their survival index was determined w.r.t. *Rv*-WT.
113 *ΔmetZ,* when compared to WT and complement strains, demonstrated a reduced ability (~40-60%) to
114 survive under all the stress conditions tested (Fig. 2A). Further, we determined intrabacterial redox

115 state using genetically encoded redox biosensor, Mrx1-roGFP2 and observed a significant rise in
116 intracellular ROS in *ΔmetZ* compared to WT strain (Fig. 2B) suggesting an inability of the strain to
117 maintain redox homeostasis possibly due to impaired mycothiol recycling. Subsequently, increased
118 levels of lipid hydroperoxides in *ΔmetZ* as opposed to WT and complement strains corroborate with
119 our findings that the absence of *metZ* in *M. tuberculosis* results in excess accumulation of intracellular
120 ROS (Fig. 2C). We then checked the role of *metZ* in the intracellular survival of the *M. tuberculosis*
121 inside the macrophages. Briefly, resting or IFN-γ induced THP-1 derived macrophages were infected
122 with H37Rv, *ΔmetZ* and the complemented strain and survival respective survival were monitored by
123 CFU plating of the macrophage lysates at day 5 post infection. We observed that *ΔmetZ* displayed a
124 reduced bacterial burden (~60%) as compared to WT and complement strains inside resting
125 macrophages, which was further significantly reduced (~48%) inside activated macrophages (Fig. 2D).
126 Since restricting the phagolysosomal fusion is a common strategy employed by the pathogen to
127 increase its chances of survival inside the cell, we checked the role of *metZ* in preventing the fusion of
128 phagolysosomes. Briefly, IFN-γ induced THP1 macrophages infected with GFP expressing wild type,
129 *ΔmetZ* and complemented strains were subsequently stained with Lysotracker. The study revealed that
130 relative to the wild type and complemented strains, *ΔmetZ* was more likely to end up in the acidic
131 compartment of the cell (Fig. 2E). Overall, the data suggests that absence of *metZ* weakens the ability
132 of *M. tuberculosis* to resist host-induced physiological stress and phagosome-lysosome fusion both
133 critical for survival of the pathogen inside the host cell.

134 **Direct sulfhydrylation pathway is essential for *M. tuberculosis* to survive under low pH**

135 The above data suggest an enhanced sensitivity of *ΔmetZ* on exposure to acidic pH. To confirm this,
136 we cultured different bacterial strains (WT, *ΔmetZ* and complement) at various pH and observed the
137 changes in growth kinetics. While the growth kinetics of all three strains were similar at neutral pH

138 (7.2), a decrease in pH led to an observable defect (pH 5.5) to complete growth arrest (pH 5.0) of the
139 *ΔmetZ* strain relative to the wild type and complemented strain (Fig. 3A and S4 A-C). Further, to
140 determine the effect of acidic pH on expression of genes involved in transsulfuration (*metB* and *metC*)
141 and direct sulfhydrylation (*metZ*), we cultured *M. tuberculosis* at pH 7.2 and pH 5.5. Relative
142 expression determined by RT-qPCR revealed that expression of *metZ* increased by ~ 12-fold upon
143 induction by acidic pH 5.5 when compared to its expression at pH 7.2 (Fig. 3B). To verify if the low
144 CFU counts at pH 5.5 (Fig. S4C) is due to bacterial killing or a consequence of metabolic slowdown,
145 we determined metabolic activity of the mycobacterial strains at pH 5.5 using Resazurin dye [22]. We
146 find that relative to the wild type and the complemented strain, *ΔmetZ* failed to change the color of the
147 dye from blue to red which corresponded to a low fluorescence readout indicating that the absence of
148 *metZ* significantly alleviated the metabolic activity of *ΔmetZ* grown in pH 5.5 (Figure 3C).
149 Furthermore, estimated ATP levels in all three strains when cultured at acidic pH 5.5 revealed that
150 *ΔmetZ* surprisingly had higher ATP levels relative to WT and complemented strains (Fig. 3D). It is
151 known that PYZ is active only at acidic pH and efficiently kills slow or non-replicating cells. We
152 hypothesized that the differences in the cytoplasmic pH will directly correlate with PYZ sensitivity.
153 As expected, we observed a ~19-fold and 4-fold increase in the sensitivity of *ΔmetZ* to PYZ treatment
154 in comparison to WT and complemented strain respectively (Fig. 3E). To confirm, if the observed
155 phenotype is a direct consequence of defect in the biosynthesis of methionine, we measured the
156 intracellular levels of methionine in H37Rv and *ΔmetZ* grown in media at both the pH. We found that
157 methionine levels were significantly lowered in WT strain when grown in acidic pH 5.5 compared to
158 bacteria grown at pH 7.2. Similarly, mutants had lower methionine levels at acidic pH in comparison
159 to mutant cells grown at pH 7.2 (Fig. 3F). Interestingly, exogenous supplementation of methionine
160 partially rescued the growth defect phenotype of *ΔmetZ* observed at pH5.5 (Fig. 3G). Interestingly, it
161 was also seen that while growing at acidic pH, *M. tuberculosis* can produce H_2S at levels significantly

162 higher than that growing at neutral pH (Fig. S5B). H_2S is a co-substrate and S-donor in the reaction
163 catalyzed by OSHS enzyme (MetZ). In sum, a defect in the methionine biosynthesis pathway at low
164 pH renders *ΔmetZ* metabolically less active thereby preventing the growth of the mutant at low pH.

165 **Molecular docking and MD simulations revealed enhanced stability of MetZ at acidic pH**

166 To enable us to perform *in-silico* molecular docking with MetZ protein (Fig. 4A), we determined the
167 binding site of O-succinyl homoserine (OSH) by focused molecular docking [23, 24] that provided the
168 final pose at the cofactor bound site. A pose with docking energy of -4.07 Kcal/mol and cluster size of
169 50 (out of 200) was found suitable at pH 7.0. While, at pH 5.5 the most likely pose showcased a docking
170 energy of -4.19 Kcal/mol with a cluster size of 80 (200). For both these poses at diverse pH, a static
171 thermodynamic quantification was carried out using MM-GBSA which was found to be -49.20
172 Kcal/mol and -56.93 Kcal/mol, respectively. Molecular Dynamics Simulation at a constant pH was
173 performed for these poses. Following the 300ns MD simulations, the protein exhibited stable RMSD
174 values at 2.98 Å and 4.34 Å at pH 7.0 and 5.5, respectively. However, significant changes were
175 observed in the stability of the substrate as well as the occupied binding site. On observing the substrate
176 in consensus with its binding site, the region was found to have higher stability and an average RMSD
177 of 1.87 Å was observed at pH 5.5 in comparison to an average of 2.71 Å at pH 7.0 (as shown in Fig.
178 4B and D). The underlying reason for this higher stability at pH 5.5 is due to the establishment of stable
179 durable bonds in the form of hydrogen bonds with residues V196, F197 and T319 and the O-atoms at
180 the terminals of the substrate. Furthermore, another factor which enhances the strength is the formation
181 of a salt-bridge with residue H220 and substrate. However, a similar configuration of H-bonds and salt-
182 bridge are not observed at pH 7.0, possibly due to conformational dynamics [25] (Fig. 4E). These
183 characteristics are a result of the change in pKa values as well as conformations of the binding site
184 forming amino acid residues. Protonation states of amino acids are highly susceptible to change in

185 environmental pH and thus, preparing the protein at pH 7.0 and 5.5 generates different acid dissociation
186 constants, which ultimately affects the bond forming tendencies of residues. The residue E165 attains
187 a pKa of 8.78 at pH 7.0 and donates a proton, forming a bond with the substrate. Similarly, D194 attains
188 a pKa of 9.11 at pH 5.5 which affects its binding to the substrate. Also, H220 is present in a protonated
189 state at a lower pH and thus involved in the formation of a Salt-Bridge with the substrate. While at pH
190 7.0, H220 remains in a deprotonated state and thus does not contribute to the stability of the binding
191 pocket at neutral pH. This showcases the importance of the acidic pH which contributes to relatively
192 greater stability of the substrate. On analysis of the binding site, we found that H220 and T319 interact
193 with the substrate at the acidic pH but they showcase conformational changes at pH 7.0 which hinders
194 their interaction. The imidazole ring sidechain of H220 rotates in anti-clockwise direction and thus
195 does not get involved in bond formation. Similarly, T319 forms H-bonds at both pH but the nature of
196 the bonds varies from transient at pH 7.0 to largely consistent at pH 5.5. Overall, conformational
197 changes in the binding site residues can be accredited for better stability at pH 5.5 The stability of the
198 protein and the substrate at acidic pH hints towards a better binding activity of the substrate. This
199 characteristic feature can be examined by performing the MM-GBSA of a few selected frames from
200 both the trajectories to compare their activity. The average binding/biological activity of the protein is
201 found to be -37.35 Kcal/mol and -59.40 Kcal/mol at pH 7.0 and 5.5, respectively (Fig. 4C). This
202 increase in the binding affinity is due to the effect of acidic pH on the protonation state as well as the
203 induced conformational changes. The docking scores at both pH 7.0 & 5.5 suggests that the residence
204 time of the substrate at the binding site must be short and the sulfur transfer reaction might be transient
205 in nature. Overall, focused docking and MD simulations revealed that although protein is stable at both
206 acidic and neutral pH, the active site of the protein holds substrate (OSH) more stably at acidic pH
207 rather at neutral pH.

208 ***metZ* mediated direct sulfhydrylation pathway is critical for methionine biosynthesis at low pH**

209 Transsulfuration pathway is well-known and characterized for methionine biosynthesis in several
210 organisms including *M. tuberculosis*. However, to confirm whether *metZ*-dependent methionine
211 biosynthesis in *M. tuberculosis* is independent of transsulfuration pathway, we knocked down
212 expression of *metB* using CRISPRi in the background of Rv-WT ($metB_{KD}$) and *ΔmetZ* ($\Delta Z::metB_{KD}$)
213 strains (Fig. 5A). Anhydrotetracycline (ATc) induced knockdown of *metB* gene in both the strains were
214 confirmed by quantifying the *metB* transcript levels by RT-qPCR (Fig. S5A). Interestingly, upon
215 induction with ATc, we find no difference in the growth of the H37Rv and $metB_{KD}$, but $\Delta Z::metB_{KD}$,
216 which upon induction by ATc behaved as a double knockout strain, was found to be defective (3.5-
217 fold at day 9) in growth even under normal pH condition (Fig. 5B). The observed growth defect could
218 be due to an obstructed methionine biosynthesis pathway which was confirmed by relative methionine
219 levels wherein we found a ~1.5-fold decrease in the intracellular methionine in $\Delta Z::metB_{KD}$ compared
220 to the $metB_{KD}$ (Fig. 5C). Further, we opined that the double mutant ($\Delta Z::metB_{KD}$) should be attenuated
221 in animal model owing to its reduced methionine levels. To test this, we infected mice with
222 mycobacterial strains (NT, $metB_{KD}$ and $\Delta Z::metB_{KD}$) and fed with doxycycline to induce CRISPRi
223 throughout the study and bacterial burden was determined by CFU plating (Fig 5D). Compared to NT
224 and *ΔmetZ,* double mutant $\Delta Z::metB_{KD}$ showed reduced bacterial burden at initial stages of infection in
225 both lungs and spleen of mice model, which however, was rescued later by week 6 (Fig. 5E). We
226 believe the presence of active methionine transporter like MetM (Rv3253) [26] could possibly be
227 involved in rescuing the growth defect phenotype of $\Delta Z::metB_{KD}$ in animal model study. Overall, the
228 data suggest that direct sulfhydrylation pathway of *M. tuberculosis* which is driven by MetZ enzyme
229 is independent of transsulfuration pathway (driven by MetB and MetC) as shutting down of both the
230 arms lead to attenuation in growth both *in-vitro* as well as *in-vivo* and reduced methionine levels.

231 **Direct sulfhydrylation pathway of *M. tuberculosis* contributes towards antibiotic persistence in**
232 **response to Bedaquiline**

233 Next, we wanted to study the role of direct sulfhydrylation pathway in regulating the drug susceptibility
234 profile of *M. tuberculosis*. We first compared the Minimum Inhibitory Concentration (MIC) of various
235 anti-TB drugs (RIF, INH, EMB and BDQ) and found that the IC50 values for each of these drugs were
236 similar for all the three strains (H37Rv, *ΔmetZ* and the complemented strain) (Fig. 6A). Further, a time-
237 kill assay was performed to determine the role of *metZ* in modulating the formation of drug-induced
238 persisters in *M. tuberculosis*. Difference in the persister formation within the strains was estimated by
239 comparing the biphasic kill curve generated by plotting the data obtained through time-kill assay.
240 Briefly, each of these cultures were treated with different antibiotics (10X MIC conc.) and the bacterial
241 survival was estimated by CFU plating of the cultures at different time points. We did not find any
242 difference in the frequency of generation of persisters between different strains treated with either RIF,
243 INH and EMB. Surprisingly, in comparison to the WT and the complemented strain, a significant
244 decrease in the persister formation was observed in *ΔmetZ* treated with BDQ (Fig 6B). Since BDQ acts
245 by restricting the ability of the pathogen to synthesize ATP, we hypothesized that the observed decrease
246 in the persister population could be a result of defect in generation of ATP in *ΔmetZ*. On the contrary,
247 our ATP depletion kinetic analysis using 2X MIC showed that BDQ treated *ΔmetZ* had higher ATP
248 levels relative to the WT and the complemented strains (Fig. 6C) suggesting that BDQ treatment led
249 to slower ATP depletion in *ΔmetZ*.

250 **Direct sulfhydrylation pathway supports the growth of *M. tuberculosis* inside the host**

251 To elucidate the role of *metZ* in mycobacterial pathogenesis, a guinea pig model of tuberculosis
252 infection was used. Briefly, guinea pigs were infected with the respective mycobacterial strains (Rv-
253 WT, *ΔmetZ* and Complement) via aerosol route. Bacterial burden in the lungs and the spleen was
254 determined by CFU plating at different timepoints post-infection. Gross and histopathological analysis
255 were performed to study the damage due to infection at the tissue level (Fig. 7A). We found that, at

256 week 4 post infection the bacterial burden in the lungs of the infected guinea pigs was ~3.7-fold and 2-
257 fold lower in *ΔmetZ* when compared to WT and Complement strains respectively. Approximately a
258 difference of ~8.9-fold was observed between bacterial burden in lungs infected with WT and *ΔmetZ*
259 at week 8 post infection. It may also be noted that no significant increment in the CFU of mutant week
260 4 through week 8 (Fig. 7B). Similarly, there were ~6-fold lesser bacilli in the spleen of *ΔmetZ* infected
261 animals opposed to WT and complement strains' infected spleen at week 4 post infection. Interestingly,
262 there was a marked decline in the recovery of colonies of *ΔmetZ* from guinea pig spleens at week 8
263 post infection. This was almost near to the limit of detection (LOD) by CFU and almost 263-fold lesser
264 bacilli than what was recovered from week 4 time point spleens (Fig. 7C). In coherence with CFU
265 burden, (Fig. 7B), we found lesser granulomatous lesions in *ΔmetZ* infected lungs as compared to WT
266 and complement strains infected lungs from week 8 lungs (Fig 7D). To visualize and quantify the
267 damage to lung tissues, H&E staining of the formalin preserved lung sections were done. Microscopic
268 examination of lung samples collected from animals infected with wild type strain revealed severe
269 granulomatous inflammation throughout the lung parenchyma. Numerous well-defined necrotizing
270 granulomas consisting of epithelioid histiocytes, perimetric cuffing of lymphocytes and plasma cells
271 aggregates and a caesious necrotic mass at the center were observed. However, lung samples from
272 animals infected with complement strain and *ΔmetZ* strain showed only non-necrotizing granulomas
273 along with multiple foci of inflammatory cells aggregates and occasional alveolar hemorrhagic patches
274 (Fig. 7E). Comparative granuloma scoring revealed the highest score for WT infected samples
275 followed by *ΔmetZ* and Complement strain infected samples (Figure 7F). Overall, the data suggests
276 that absence of *metZ* gene in *M. tuberculosis* impedes the ability of the pathogen to replicate and
277 survive inside the host indicating *metZ* (or direct sulfhydrylation) for methionine biosynthesis is
278 required for survival inside host at later stages of infection.

279 ***metZ* is involved in methionine biosynthesis in *M. tuberculosis* at acidic pH**

280 We hereby summarize that when *M. tuberculosis* infects macrophage, it passes through a series of
281 compartments starting from phagosome where pH is essentially ~6.5 and the bacteria is in replicating
282 state, with enough nutrients (including methionine). Further, as host immunity kicks in and IFN-γ
283 induces accumulation of ROS, RNS and subsequently, phagosome maturation leading to drop in pH to
284 5.5 and beyond, conditions are non-replicating for *M. tuberculosis* and host begins to quench nutrients
285 from bacteria as means to impose restriction on the trapped bacteria. At this stage bacteria undergoes
286 several transcriptional and metabolic changes to sustain the host induced insults, one of these includes
287 induction of *metZ* expression that help bacteria survive these stress conditions and helps maintain
288 methionine levels by utilizing host produced H_2S which acts as co-substrate for methionine
289 biosynthesis in acidic micro-environment and helps bacteria maintain recycling of ATP, mycothiol and
290 its metabolic activity going (Figure 8).

291

292 **Discussion**

293 *M. tuberculosis*, adapts to various conditions within macrophages, resulting in the differential
294 expression of proteins that support homeostasis. Under such circumstances, the pathogen needs to
295 evolve and device a mechanism to efficiently regulate the flux of cysteine towards either biosynthesis
296 of methionine and/or mycothiol. Cysteine, in addition to other metabolites, is a key amino acid essential
297 for biosynthesis of both methionine and mycothiol in mycobacteria. *M. tuberculosis* enhances the
298 biosynthesis of cysteine to most possibly to compensate for the increase in the flux of cysteine towards
299 generating the thiol-active metabolites (mycothiol, ergothionine, NAD+, etc.) essential for maintaining
300 the redox balance in conditions with heightened levels of ROS, RNS [27] and upon exposure to acidic
301 pH [28]. Similar findings in *E. coli* have been reported that growing demand of cytosolic redox
302 glutathione under higher oxidative stress boosts the synthesis of cysteine [29]. We, in the current study,
303 have used a combination of genetics and computational biology-based tools to probe the role of *metZ*

304 mediated direct sulfhydrylation pathway in *M. tuberculosis*. We found that MetZ dependent direct
305 sulfhydrylation is induced by several folds at acidic pH. Disrupting this pathway in *M. tuberculosis*
306 results in a decrease in methionine at low pH. Finally, we demonstrated that MetZ dependent direct
307 sulfhydrylation is required for growth of *M. tuberculosis* inside the host at later stages of infection.

308 In contrast to an earlier report [19], *metZ* was found to be dispensable for growth of *M. tuberculosis* on
309 cholesterol. The conditional essentiality phenotype observed for *ΔmetZ* under low pH further suggests
310 that the observed essentiality of *metZ* for growth on cholesterol was a result of relatively low pH growth
311 conditions used in that study. Cysteine being the common precursor for the generation of both the
312 methionine and the mycothiol, the observed imbalance in the redox homeostasis in *ΔmetZ* could be
313 attributed to the inefficient recycling of mycothiol due to a major shift of the cysteine pool towards
314 methionine biosynthesis. *M. tuberculosis metZ* (*Rv0391*) gene encodes a probable OSHS catalyzing
315 direct conversion of OSH to homocysteine using soluble H_2S instead of cysteine as S-donor. Given the
316 crucial role of methionine in bacterial physiology, there has been a gap in our understanding of the
317 rationale of harboring multiple methionine biosynthesis pathways and their role in maintaining
318 methionine homeostasis critical for the survival of *M. tuberculosis* in a nutrient deprived *in-vivo* growth
319 environment. Interestingly, other than maintaining the redox homeostasis, our data underscores the role
320 of methionine biosynthesis, through direct sulfhydrylation pathway, in regulating the cytosolic pH and
321 metabolism. The inability of the *ΔmetZ* to regulate the intracellular pH homeostasis impedes the ability
322 of the pathogen to utilize the cellular ATP rendering the pathogen metabolically less active. Similar
323 findings have been reported in *E. coli* previously where antibiotic induced oxidative stress led to
324 increased levels of intracellular ATP which is a consequence of non-utilization rather than over-
325 production [30]. This explains increased levels of ATP in *ΔmetZ* at acidic pH which is a consequence
326 of metabolic slowdown at acidic pH. The enhanced susceptibility of *ΔmetZ* to pyrazinamide (PYZ)
327 further confirms the presence of a relatively acidic cytosol and accentuates the role of *metZ* in

328 maintaining the pH homeostasis in *M. tuberculosis*. In an *ex-vivo* setting, IFN-γ induction leads to the
329 acidification of cellular compartments where the internalized bacteria is trapped and maintained at low
330 pH. As a consequence of this, *ΔmetZ* replication inside resting as well as activated macrophages was
331 reduced which was because of the comparatively higher co-localization of *ΔmetZ* mutant to acidic
332 compartments of the macrophages as revealed by confocal microscopy. Similar to our findings, other
333 studies have also observed that enhanced susceptibility to either acidic pH or oxidative stress results in
334 increased killing due to higher co-localization with acidic compartments of the macrophages [31-33].
335 Our data provides mechanistic understanding of the methionine starvation associated susceptibility in
336 *M. tuberculosis* previously reported by several groups [5, 11]. The presence of both transsulfuration
337 and direct sulfhydrylation pathway for the biosynthesis of methionine in *M tuberculosis* is indeed
338 intriguing. Although both the pathways demonstrate redundancy at normal pH, our qPCR data along
339 with previous studies categorically indicate that enzyme responsible for carrying out direct
340 sulfhydrylation is over-expressed in *M tuberculosis* upon induction with acidic pH [32, 34, 35]. These
341 findings are corroborating well with our pH dependent molecular dynamics simulation studies which
342 suggested that the binding affinity between substrate and MetZ active site is more strong at low pH.
343 The thorough pH-dependent MD simulations provide structural insights in terms of distinct behavior
344 as how pH and protonation states of key residues alter the interaction networks particularly hydrogen
345 bonding and electrostatic interactions within the binding site residues of the protein, leading to
346 significant changes in the conformation. The change in hydrogen bonding network identified as a
347 determinant which majorly impacts the change in binding affinity of the substrate. A comparative
348 analysis between two pH was evaluated in terms of MetZ structural stability using metrics such as root-
349 mean-square deviation (RMSD) and thermodynamic changes that further confirm the pH-dependent
350 behavior, indicating that *metZ*-mediated direct sulfhydrylation becomes the major methionine
351 producing pathway of *M. tuberculosis* under low pH.

352 We further confirm that *M. tuberculosis* strain that lacks both transsulfuration and direct
353 sulfhydrylation pathways (*ΔmetZ/metB*$_{KD}$) fail to generate methionine and demonstrate methionine
354 auxotrophy under *in-vitro* growth conditions implying that both the pathways are independent of each
355 other. Surprisingly, in comparison to *in-vitro* growth condition, the growth defect observed in
356 *ΔmetZ/metB*$_{KD}$ under *in-vivo* growth condition, although significant, was less pronounced. This could
357 be attributed to the fact that the pathogen is known to harbor potential methionine transporter encoded
358 by *Rv3253c* (*metM*) [26] which helps the pathogen salvage methionine from the host. It has also been
359 shown previously that *M. tuberculosis* has an ability to produce H_2S – a gaseous signaling molecule
360 upon induction with acidic pH (Fig. S5B) and [14] probably as a mechanism to counteract increasing
361 ROS and dropping metabolic potential of the cells. Further, it has also been shown that H_2S at sub-
362 inhibitory levels in *M. tuberculosis* have a positive effect on mycobacterial electron transport chain
363 (ETC) and this effect is reversible [36, 37]. Additionally, host produced H_2S in response to *M.*
364 *tuberculosis* infection and have a positive effect on bacterial replication such that *M. tuberculosis*
365 replication was hampered when host's ability to generate H_2S was abrogated either by genetically
366 knocking out enzymes responsible for H_2S generation – CSE and CBS (among others) or by using
367 pharmacological inhibitors of the same [36, 38, 39]. Co-incidentally, through literature it has also been
368 extensively established that sulfhydrylases in general, use H_2S as S-donor to either synthesize cysteine
369 or, in this case, MetZ produces homocysteine, hence, methionine.

370 Development of antibiotic persistence in bacteria is a major culprit responsible for the failure of anti-
371 TB regimen. Frequency of generation of persister population can be quantified by performing time-kill
372 assay by treating different culture at high dosage of antibiotic (5-10X MIC). A biphasic kill kinetics is
373 indicative of drug persistence [40]. Our time-kill experiments suggest that the absence of direct
374 sulfhydrylation pathway in *ΔmetZ* prevents the BDQ specific generation of antibiotic persistence in *M.*
375 *tuberculosis*. Intriguingly, in spite of higher cytosolic ATP levels relative to the wild type, *ΔmetZ*

376 demonstrated a decrease in the frequency of BDQ specific persisters formation. This is similar to
377 previous study where authors have reported *ΔpckA* strain maintained higher ATP levels even upon
378 treatment with BDQ grown in presence of acetate which promoted persister formation in *ΔpckA*.
379 However, as opposed to our findings, they demonstrated that *ΔpckA* had increased drug tolerance and
380 more ATP levels in acetate medium [41]. In sum, apart from maintaining methionine levels at acidic
381 pH, direct sulfhydrylation pathway also modulate BDQ specific generation of antibiotic persistence
382 during infection. Future studies on understanding this complex phenotype will help us design strategy
383 to prevent the development of BDQ resistance in tuberculosis. It was also found that *metZ* is required
384 for maintenance of *M. tuberculosis* infection in guinea pig model of tuberculosis infection, as indicated
385 by a lowered CFU burden at week 8 post-infection and severe attenuation in the spleen as well. Spleen
386 is known to have a high iron content, which itself is responsible for the generation of ROS via Fenton
387 chemistry. Given the susceptibility of the *metZ* mutant to oxidative stress, we find a very low bacterial
388 count in the spleen at week 8 post-infection. This suggests that *metZ* supports methionine biosynthesis
389 and hence bacterial survival in a nutrient deprived and low pH niche inside the host.

390 The presented data therefore, suggest that *M. tuberculosis* is short of methionine at acidic pH when
391 trapped inside phagolysosome. At this stage, expression of *metZ* is induced several folds as opposed to
392 *metB* and *metC*. Absence of direct sulfhydrylation pathway curtails the growth of Mtb at acidic pH by
393 significantly reducing the metabolic activity together with decrease in the ability to utilize the cellular
394 ATP. Further, such conditions arise around 3–4-week post infection in animal model which is marked
395 by onset of IFN-γ mediated bacterial control where antimicrobial mechanisms are at peak posing
396 challenge to bacteria in the form of ROS, RNS, acidic pH and increasing H_2S biogenesis. Concordantly,
397 *metZ* null mutant was susceptible to all these stresses *in-vitro*, verifying our findings. Our results,
398 hence, indicate that *M. tuberculosis* adapts to the decreasing pH in its surroundings to maintain
399 methionine biosynthesis through direct sulfhydrylation using exogenous and perhaps endogenous H2S

400 as S-donor. This makes MetZ an interesting drug target that can be aimed in combination with anti-TB
401 drugs to improve their efficacy. A pharmacological inhibitor of MetZ should be able to inhibit
402 methionine biosynthesis in the bacteria trapped inside a non-replicative condition (i.e. phagolysosome)
403 characterized by exceedingly low pH ~4.5-5.5. Another strategy could be using small molecules that
404 could drop intrabacterial pH of *M. tuberculosis* [42] in combination with pharmacological inhibitors
405 of MetZ. This would ensure bacterial growth arrest due to reduced Intrabacterial pH and block
406 methionine biosynthesis at the same time by inhibiting MetZ.

407

408 **Materials and Methods**

409 **Bacterial strains**

410 Knockout strain of *metZ* gene *(rv0391)* was generated in the genetic background of wild type
411 *M. tuberculosis* H37Rv by genetic recombineering. Briefly, a gene-specific allelic exchange
412 substrate (AES) harboring 1kb sequences of target gene upstream and downstream homology
413 flanking Hygromycin resistance gene cassette was constructed in the suicidal vector pJM1. AES
414 was transformed into H37Rv (wild-type) strain overexpressing Phage Che9c RecET proteins to
415 facilitate recombination. Recombinants with the Hyg^r gene were selected over Hyg plates and
416 screened using gene-specific PCR. The marked mutant thus prepared was unmarked to excise out
417 Hyg resistance cassette using Cre-recombinase expressed from plasmid pCre-SacB-Zeo. Unmarked
418 mutant was confirmed by PCR and RT-qPCR to confirm loss of gene as well as transcripts of metZ
419 gene. Unmarked mutant was then transformed with plasmid expressing a functional copy of *metZ*
420 gene under P_{myc1}*tetO* promoter replicating either episomally or integrated to generate genetic
421 complementation strain (denoted as *ΔmetZ Comp*). Bioluminescent mycobacterial strains were
422 generated by transforming respective mycobacterial strains (**List of Strains, Appendix-I**) with

423 integrative plasmid expressing *luxABCDE* operon (Addgene # 26161) [43] with slight
424 modifications [44]. Strains were checked for bioluminescence and a luminescence vs CFU plot was
425 prepared to determine linear relation between luminescence and CFU based read-outs of bacterial
426 viability for lux-based mycobacterial strains (Fig S3A).
427
428 **Media and cultural conditions**
429 The bacterial strains were maintained as frozen glycerol stocks at -80°C. Whenever required, the
430 stocks were thawed and diluted 1:500 in 7H9 (Difco, BBL) medium supplemented with OADS and
431 0.01% Tween 80. Bacterial enumeration was done on 7H11 (Difco BBL) agar plates supplemented
432 with OADS. Kanamycin (Sigma), 25µg/ml, Hygromycin (Sigma), 50µg/ml and Zeocin
433 (Invitrogen), 25µg/ml were used whenever required. For media with no carbon source, 7H9 base
434 medium was prepared without glycerol and OADS (or ADS) enrichment and later supplemented
435 with desired C-sources and 0.05% tyloxapol. 100mM stock of Cholesterol (Sigma) was prepared
436 by heating cholesterol in Tyloxapol (Sigma): Ethanol (Merck) mix (1:4) at 80°C for 30 mins [45].
437 When required, cholesterol was diluted to desired concentration (200µM) in 7H9 base medium
438 wherever specified. Likewise, glycerol (Sigma) was used at final concentration 0.1% v/v and
439 sodium propionate (Sigma) was used at concentration of 10µM (0.1%) for growth kinetics studies.
440 For pH dependent growth kinetics experiments, 7H9 base medium was prepared, supplemented
441 with 0.2% glycerol (v/v) and ADS acidified to desired pH using HCl. Phosphate buffered saline
442 (PBS) was used at 1X concentration supplemented with tyloxapol (0.05%) whenever mentioned.
443 Bacterial enumeration by CFU was done on 7H11 agar plates supplemented with OADS, wherever
444 mentioned. Colonies were counted after 21 days of incubation. Anhydrotetracycline, ATc (Caymen)
445 was used at 200 ng/mL concentration, unless mentioned otherwise.
446

447 **CRISPRi knockdown**

448 For transcriptional knockdown of *metB (Rv1079)* using CRISPR interference (CRISPRi), target
449 specific sgRNA was cloned into *BsmBI* (NEB) digested backbone plJR965 (Addgene # 115163) to
450 generate knockdown construct. Knockdown construct was transformed into *Rv*-WT and *ΔmetZ*
451 strains. To achieve knockdown of the target genes, cells were grown to mid-log phase and diluted
452 back to OD 0.01 in fresh culture medium with or without ATc. Growth was monitored by measuring
453 OD of the cultures. Further, expression of target genes was quantified by qPCR to determine the
454 levels of knockdown.

455

456 **RT-qPCR**

457 Total RNA was isolated from the respective bacterial strains under specific conditions using Trizol
458 (TaKaRa) according to the manufacturer's protocol. Briefly, bacterial cells were washed with 1X
459 PBS and resuspended in Trizol. Cells were lysed by bead-beating using 0.22µM sized zirconia beads
460 via 5 cycles with intermittent cooling step of 1 minute. Further, RNA was extracted and precipitated
461 using chloroform-isopropanol treatments. Total RNA thus prepared was treated with Turbo DNaseI
462 (Ambion) to digest away the DNA contamination. 3000 µg equivalent DNase treated RNA was
463 used to prepare cDNA using SuperScript IV Reverse Transcriptase (Invitrogen). Finally, 1µg
464 equivalent cDNA was used to set up qPCR reactions with SYBR (TaKaRa). *sigA* was used as
465 internal control and $\Delta\Delta C_t$ method [46] was used determine relative gene expressions w.r.t. specified
466 control conditions. For qPCR at acidic pH, *icl1* was used as positive control.

467

468 **Growth kinetics**

469 Auto-bioluminescent bacterial strains were grown till OD 0.5 (mid-log phase) and washed once
470 with 1X PBST to remove the spent media. The cells were resuspended in 1X PBST and diluted back

471 to an OD of 0.01 in 7H9 base medium supplemented with different carbon sources – glycerol
472 (0.1%), cholesterol (200µM) or propionate (10mM) for C-source dependent growth kinetics. For
473 pH dependent growth kinetics, bacterial cells were diluted back to an initial OD of 0.05 in 7H9
474 medium (supplemented with ADS and 0.2% glycerol) acidified to different pH – 7.2, 6.5, 5.5 and
475 5.0. Whenever required, L-methionine (50µg/ml, Sigma) was added to the cultures. The growth was
476 monitored by measuring OD and/ or auto-bioluminescence using a Multimode Microplate reader
477 (SpectraMax Pro ID3, Molecular Devices). At times, bacterial growth was also determined by CFU
478 at indicated time points by plating aliquots of cultures and plating appropriate dilutions on 7H11
479 agar plates.
480
481 **Physiological stress survival assay**
482 Bacterial strains were grown till OD 0.5 (mid-log phase) and washed once with 1x PBST. Aliquots
483 of 2ml cell suspensions equivalent to OD 0.2 were treated with 0.5mM H_2O_2 (oxidative stress),
484 200µM Deta-NO (nitrosative stress), 0.01% SDS (membrane stress), PBST (nutrient starvation
485 stress), Phosphate citrate buffer, pH 5.5 (acidic stress) *in-vitro*. The survival of the respective strains
486 was determined by CFU plating at indicated time points and calculating survival index (i.e., CFU
487 of strain/ CFU of Rv-WT).
488
489 **Drug susceptibility (MIC determination)**
490 Auto-bioluminescent bacterial strains were grown till OD 0.5 (mid-log phase) and washed with 1x
491 PBST. Anti-TB drugs (RIF, INH, BDQ, EMB, CFZ and PYZ) were serially diluted on a 10-points,
492 2-fold format and added to the 96-well plates (SPL). Cells were added at final density of OD 0.01
493 to the wells containing drugs and incubated at 37°C for 3 days as described previously [47]. Finally,

494 luminescence was recorded as an indicator of bacterial viability which was expressed as dose-
495 response curves and IC_{50} were calculated using non-linear regression analysis in GraphPad Prism.
496
497 **Kill kinetics**
498 Bacterial strains were grown till OD 0.5 (mid-log phase) and washed with 1x PBST. Aliquots of
499 cell suspensions (2ml) at bacterial density of OD 0.2 were treated with 10X MIC concentrations of
500 anti-TB drugs (Rif, Inh, Emb and Bdq) for mentioned time. Bacterial survival was determined by
501 CFU enumeration at indicated time points.
502
503 **Methionine estimation**
504 Log-phase cultures of mycobacterial strains were washed with 1X PBST and transferred to 7H9
505 medium maintained at pH 7.2 or 5.5 at an OD 0.4. Cultures were allowed to grow for 6 days after
506 which they were washed with 1X PBS once followed by washing with chilled methanol. Cells
507 equivalent to OD 1 (~$3x10^8$ cells/mL) were lysed in 1 ml extraction buffer (Acetonitrile:Methanol:
508 water:: 2:2:1) by bead beating with intermittent cooling of 1 min per cycle. Lysates were clarified
509 by spinning at 13,000 rpm, 10 mins at 4°C. The clarified supernatants were filtered through 0.22-µ
510 filters and dried by speed vac to evaporate the extraction buffer. Dried pellets were resuspended in
511 methanol:water (1:1) + 0.1% formic acid and vigorously mixed. Finally, 10µL of the reconstituted
512 samples were run on Hypersil Gold C8 column (100 x 2.1mm) with 0.1% formic acid in water as
513 mobile phase A and 0.1% formic acid in acetonitrile as mobile phase B on SCIEX 6500+ QTRAP
514 and peak and retention time was matched with standard (Methionine) across all the samples. Peak
515 intensities were normalized to CFU of the respective samples.
516
517 **Total ATP estimation**

518 Cultures of Rv-WT, *ΔmetZ* and Complement were grown at acidic pH 5.5 till OD 0.5 (mid-log
519 phase) and washed with 1X PBST. Cells were resuspended in 1000µL 1X PBST (with Protease
520 Inhibitor Cocktail) and lysed by 5 cycles: 45 seconds of bead beating with intermittent cooling on
521 ice. Lysates were passed through 0.5-µ sized filters to remove any bacterial cells or debris. 50µL of
522 clarified lysates were transferred to a 96-well plate (white, flat-bottom, SPL) and mixed (1:1) with
523 BacTiter-Glo (Promega) reaction buffer followed by incubation at 37°C for 30 minutes. 1X PBS
524 was used as blank to cancel out the background signals from the samples. Luminescence was
525 recorded using a Multimode Microplate reader (SpectraMax Pro ID3, Molecular Devices).
526 Normalization was done using total protein content of the respective samples and ATP levels were
527 expressed as relative units w.r.t. Rv-WT strain. For ATP estimation of BDQ treated cultures, 0.4
528 OD bacterial suspensions (2ml) of the respective strains were treated with 2X MIC concentration
529 of BDQ for the indicated time-points and samples were prepared as described above.
530
531 **Metabolic activity**
532 Auto-bioluminescent mycobacterial strains were grown till OD 0.5 (mid-log phase) and washed
533 with 1X PBST to remove the spent media. Cells were resuspended in 1X PBST and re-diluted to an
534 OD of 0.4 in media acidified to required pH (pH 5.5). 100µL of these suspensions were added to a
535 96-well plate (white, flat-bottom, SPL) containing 7H9 (ADS + 0.1% glycerol, pH 5.5) and serially
536 diluted (2-fold). The periphery wells were filled with sterile medium to prevent desiccation. The
537 plate was incubated at 37°C for 5 days after which 20µL of PrestoBlue (Thermo) was added to each
538 well followed by an additional incubation of 2 days to allow development of color. After 2 days of
539 incubation, luminescence read-out was taken and contents of the wells were transferred to a clear
540 bottom black plate followed by recording fluorescence of AlamarBlue at 560(ex)/ 590(em). Ratio
541 of Fluorescence/Luminescence was calculated to determine metabolic activity per cell.

542

543 **Intracellular redox state**

544 Rv-WT, *ΔmetZ* and Complement strains were transformed with plasmid encoding redox biosensor,
545 Mrx1-roGFP2 as described previously [48]. Cells were grown to OD 0.5 and washed with 1X PSBT
546 and resuspended in PBST in MCTs. Rv-WT cells in respective tubes were treated with either 100µM
547 CHP or 100µM DTT as control groups for oxidized and reduced conditions respectively. Further,
548 cells were transferred to 96-well plates (clear bottom, black wells) and excitation at 430 and 490 nm
549 while emission at 510 nm was recorded. Ratio of fluorescence at 390 nm/490 nm were compared to
550 determine intracellular redox state of the cells.

551

552 **Lipid hydroperoxidation assay**

553 Total lipids were extracted from the respective bacterial strains as described previously [49]. Briefly,
554 bacterial cells were grown to an OD 0.8-1.0 and pelleted down. Pellets were suspended in
555 methanol:chloroform (2:1), 6 ml overnight at 37°C to extract total cellular lipids. Next day, cells
556 were spun down and supernatants were collected. Supernatants having total cellular lipids were
557 further precipitated by saturating the supernatants with 0.8% KCl. The lower phase was collected
558 and dried in glass vials to evaporate the solvents and concentrate the lipids. Dried lipids were
559 resuspended in 1 ml chloroform (Sigma) and used for FOX2 assay for determining lipid
560 hydroperoxidation in the extracted lipids as described elsewhere [50]. Briefly, 200µL of the
561 concentrated lipids were mixed with 1000µL FOX2 reagent in MCTs in dark for 1hr. Samples were
562 transferred to a 96-well plate and read out at 560 nm.

563

564 **Intracellular sulfide estimation**

565 Total sulfide estimation was performed as described previously [51] [37]. Briefly, Rv-WT, *ΔmetZ*
566 and Complement strains were grown to OD 0.5 (mid-log phase) in regular 7H9 medium
567 supplemented with OADS and 0.01% Tween 80. Cells equivalent to OD 0.5 were inoculated into
568 7H9 medium supplemented with ADS and 0.01% tyloxapol at pH 7.2 and pH 5.5. After 4 days of
569 incubation, the cultures were pellet down and washed with 1X PBST to remove spent media. Pellets
570 were resuspended in the same media with respective pH 7.2 and 5.5 at an OD 0.4. 100µL of the cell
571 suspensions were added to 96-well plate and mixed with 100µL 2X Bismuth chloride buffer.
572 Following an incubation of 4 hours at 37°C, colorimetry was done at 405nm. The values were
573 normalized to culture OD to determine relative sulfide levels in the respective strains at two different
574 pH.
575
576 **Macrophage infection**
577 THP-1 monocytic cells were grown in RPMI medium (Lonza) supplemented with 10% fetal bovine
578 serum (FBS, Invitrogen). Further, cells were seeded at a density of $5x10^5$ cells/ well in a 12-well
579 plate (Corning) and matured for 24 hours with PMA (25ng/mL, Sigma) followed by a rest of 24
580 hours. Whenever required, cells were activated with IFN-γ (10ng/ml, Peprotech) for 16 hrs before
581 infection. Single cell suspensions of the bacterial strains (Rv-WT, *ΔmetZ* and complement) were
582 prepared by soft-spin method as described [44] and used for infecting resting or activated
583 macrophages at an MOI of 1. Bacteria were allowed to infect the cells for 4 hours after which,
584 extracellular bacteria were washed off by three washes with pre-warmed PBS (Gibco). At indicated
585 time points, macrophages were lysed with 1X PBS + 0.01% Triton X-100 to release intracellular
586 bacterial cells. Lysates were serially diluted and plated for bacterial enumeration.
587
588 **Confocal Microscopy**

589 THP-1 macrophages were seeded on glass coverslips in a 24-well plate ($5x10^5$ cells/well) and were
590 activated by 10ng/ml of human IFN-γ (Peprotech, USA) for 16 hours before infection. Activated
591 THP-1 cells were infected with mycobacterial strains (Rv-WT, *ΔmetZ* and Complement) harboring
592 Live-Dead reporter plasmid [52] constitutively expressing mEmerld at an MOI of 10. After 4 hours
593 of infection, the cells were washed thrice with 1X PBS to remove the extracellular bacteria and
594 replenished with fresh media. Subsequently, after 24 hours post infection, cells were incubated with
595 50nM LysoTracker Red DND-99 (Invitogen life Technologies, CA, USA) in complete RPMI media
596 for 30 minutes at 37°C with 5% CO2 and later fixed with 4% paraformaldehyde in 1X PBS.
597 Coverslips were mounted with ProLong Diamond antifade with DAPI (Molecular Probes by Life
598 Technologies, CA, USA). Finally, slides were imaged by Olympus Confocal Laser Scanning
599 Microscope (CLSM). Later, GFP-expressing mycobacteria that colocalized with LysoTracker Red
600 was determined by analyzing the ~ 100 phagosomes and co-localization index was determined.
601

602 **Animal Infection**

603 *In-vivo* experiment in this study was performed with approval from Institutional Animal Ethics
604 Committee (IAEC Approval No: IAEC/THSTI/165) as per guidelines laid by Committee for the
605 Purpose of Control of Experiments on Animals (CPCEA), Government of India. Briefly, bacterial
606 suspensions of respective strains at a density of 10^8 cells/mL were prepared in normal saline and
607 guinea pigs (Duncan Hartley) were infected via aerosol route using Inhalation Exposure System
608 (Glas-Col). Animals were euthanized at indicated time points, organs were harvested and bacterial
609 burdens were determined by CFU plating. Histopathological damage to the lung tissue was
610 determined by H&E staining of lungs fixed in 5% paraformaldehyde followed by granuloma scoring
611 of the infected lung tissue.

612 **CRISPRi mediated *in-vivo* fitness**

613 The experiment was performed with approval from Institutional Animal Ethics Committee (IAEC
614 Approval No: IAEC/THSTI/196) as per guidelines laid by Committee for the Purpose of Control of
615 Experiments on Animals (CPCEA), Government of India. Briefly, bacterial suspensions of respective
616 strains (NT and *ΔZ::metB*$_{KD}$) at a density of $3x10^8$ cells/mL were prepared in normal saline and
617 BALB/c mice were infected via aerosol route using Inhalation Exposure System (Glas-Col). To
618 induce CRISPRi mediated gene silencing of *metB* in *ΔZ::metB*$_{KD}$ strain, doxycycline (1 mg/ml) was
619 administered to mice via oral route at indicated time points [**53**]. NT (non-targeting CRISPRi strain)
620 was maintained with doxycycline as control which is isogenic to Rv-WT. Animals were euthanized
621 at indicated time points, organs (lungs and spleens) were harvested and bacterial burden were
622 determined by CFU plating.

623

624 **Bioinformatics analysis**

625 MetZ protein sequence was retrieved from Mycobrowser
626 (https://mycobrowser.epfl.ch/genes/Rv0391) and the cluster of orthologous groups analysis (COG)
627 was performed using Eggnog v5 [54]. Further, a multiple sequence alignment of the protein sequence
628 from members of *Mycobacterium* genus (*M. tuberculosis, M. bovis, M. canettii, M. marinum, M.*
629 *leprae* and *M. smegmatis*) along with gram negative (*Pseudomonas aeruginosa*) and gram-positive
630 bacterium (*Corynebacterium glutamicum* and *Rhodococcus*) was performed using Clustal W [55] to
631 identify common domains and motifs amongst the protein sequences.

632

633 **Molecular docking and molecular dynamics simulations**

634 For system preparation, the crystal structure of putative O-succinylhomoserine sulfhydrylase of *M.*
635 *tuberculosis* was retrieved from RCSB PDB [56] (PDB-ID: 3NDN [57]). The protein has 4 chains and

636 exists in a homo-tetramer form. The receptor has a covalently bound pyridoxal-5-phosphate attached
637 to a modified lysine (K219). The substrate, O-succinyl homoserine, was retrieved from PubChem
638 (PubChemCID 439406). The substrate undergoes a sulfur transfer reaction in the presence of
639 pyridoxal-5-phosphate forming L-homocysteine which takes part in the methylation cycle. The
640 receptor protein was optimized and then minimized using the OPLS3 force field of Protein Preparation
641 Wizard module [58] of Schrodinger suite. Next, Binding Site Identification was done using Autodock
642 4 [59] wherein blind docking of the substrate in the presence and absence of the cofactor to identify
643 the possible binding site was performed. Autogrid4 was used to build a 126x126x126 points grid map
644 with a spacing of 0.586 angstrom and positioned at the center of mass of the receptor protein. The
645 Lamarckian genetic algorithm was employed to generate 200 runs. On docking the substrate in the
646 presence of the cofactor, no suitable results were produced. However, docking in the absence of the
647 co-factor resulted in comparatively higher binding affinity and a larger cluster size. Focused docking
648 on the identified site was also carried out by generating a grid map of 40x40x40 units with a spacing
649 of 0.375 A and 17X20X22 as grid center coordinates. MM-GBSA of few conformers based on their
650 binding affinity and cluster size was done using Prime module [60] of maestro. Finally, the lowest
651 energy conformations of the substrate were subsequently used for constant pH MD. Further, Constant
652 pH Molecular Dynamics Simulation (MDS) was performed with the Desmond [61] module from
653 Schrodinger suite. Both systems were protonated at pH 5.5 and 7.0, respectively, and minimized with
654 OPLS- all Atom force fields and solvated with the predefined TIP3P water solvent model. The
655 complexes were placed in the orthorhombic periodic boundary conditions to specify the shape and size
656 of the repeating unit buffered at 12 A distances. 4 Na+ and 9 Na+ ions were added to both the systems
657 respectively, to neutralize the systems. The NPT ensemble was employed for the simulation with a
658 timestep of 0.002 ps. The simulation was carried out for a total of 300 ns for each system and the
659 coordinates were saved at intervals of 20 ps to generate 15000 frames. Also, the protein was simulated

660 without the substrate at the two pH values. The post-processing of MD simulation trajectories was
661 carried out using VMD [62]. The root-mean-square-deviation and fluctuation were measured for the
662 protein, substrate and cofactor. Lastly, for thermodynamics analysis of the system we performed
663 Molecular Mechanics Generalized Born Surface Area (MM-GBSA) analysis to evaluate the MD
664 trajectories using Schrodinger software. To effectively encompass the thermodynamic properties,
665 every 500th frame was selected for MM-GBSA analysis.

666

667 **Statistical Analysis**

668 The data values are represented as mean ± SEM of the two-three independent experiments. Statistical
669 comparisons have been made with Rv-WT in most cases unless mentioned otherwise. GraphPad
670 Prism (ver 9.0) has been used for statistical analysis of all data with suitable statistical tests mentioned
671 with figure legend.

672

673 **Conflict of Interest**

674 The authors declare no conflict of interests

675

676 **Acknowledgments**

677 Authors acknowledge THSTI for infrastructural support, Department of Biotechnology, Government
678 of India for funding, Experimental Animal Facility for supporting animal experimentations and BSL-
679 3 facility for conducting all *M. tuberculosis* related experiments. Technical support of Mr. Surjit Yadav
680 is duly acknowledged. We acknowledge the Multi-Omics facility for LC-MS based experiments.

681

682 **Funding**

683 This study was supported by the grant (No. EM/Dev/SG/212/7864/2023) from the Indian Council of
684 Medical Research (ICMR), Government of India and intramural funding by BRIC-THSTI to A.K.P.
685 and are duly acknowledged. VKN is supported by a research fellowship from ICMR (3/1/3/JRF-
686 2018/HRD-043/64467).

687

688 **Supplementary material**

689 1. Table S1: List of plasmids and constructs used in the study

690 2. Table S2: List of bacterial used in the study

691 3. Table S3: List of primers used in the study

692

693 **List of relevant references:**

694

695 1. WHO, *World TB report 2022.* 2023.

696 2. Yelamanchi, S.D. and A. Surolia, *Targeting amino acid metabolism of Mycobacterium*
697 *tuberculosis for developing inhibitors to curtail its survival.* IUBMB Life, 2021. **73**(4): p. 643-
698 658.

699 3. Adams, J.M. and M.R. Capecchi, *N-formylmethionyl-sRNA as the initiator of protein synthesis.*
700 Proc Natl Acad Sci U S A, 1966. **55**(1): p. 147-55.

701 4. Kim, J.M., et al., *Formyl-methionine as an N-degron of a eukaryotic N-end rule pathway.*
702 Science, 2018. **362**(6418).

703 5. Berney, M., et al., *Essential roles of methionine and S-adenosylmethionine in the autarkic*
704 *lifestyle of Mycobacterium tuberculosis.* Proc Natl Acad Sci U S A, 2015. **112**(32): p. 10008-
705 13.

706 6. Chaton, C.T., et al., *Structural analysis of mycobacterial homoserine transacetylases central*
707 *to methionine biosynthesis reveals druggable active site.* Sci Rep, 2019. **9**(1): p. 20267.

708 7. Chaudhary, D., et al., *Identification of small molecules targeting homoserine acetyl transferase*
709 *from Mycobacterium tuberculosis and Staphylococcus aureus.* Sci Rep, 2022. **12**(1): p. 13801.

710 8. Berger, B.J. and M.H. Knodel, *Characterisation of methionine adenosyltransferase from*
711 *Mycobacterium smegmatis and M. tuberculosis.* BMC Microbiol, 2003. **3**: p. 12.

712 9. Venos, E.S., et al., *Branched-chain amino acid aminotransferase and methionine formation in*
713 *Mycobacterium tuberculosis.* BMC Microbiol, 2004. **4**: p. 39.

714 10. Lee, H.S. and B.J. Hwang, *Methionine biosynthesis and its regulation in Corynebacterium*
715 *glutamicum: parallel pathways of transsulfuration and direct sulfhydrylation.* Appl Microbiol
716 Biotechnol, 2003. **62**(5-6): p. 459-67.

717 11. Hasenoehrl, E.J., et al., *Derailing the aspartate pathway of Mycobacterium tuberculosis to*
718 *eradicate persistent infection.* Nat Commun, 2019. **10**(1): p. 4215.

719 12. Smith, D.A., et al., *Characterization of auxotrophic mutants of Mycobacterium tuberculosis*
720 *and their potential as vaccine candidates.* Infect Immun, 2001. **69**(2): p. 1142-50.

721 13. Wheeler, P.R., et al., *Functional demonstration of reverse transsulfuration in the*
722 *Mycobacterium tuberculosis complex reveals that methionine is the preferred sulfur source for*
723 *pathogenic Mycobacteria.* J Biol Chem, 2005. **280**(9): p. 8069-78.

724 14. Mishra, R., et al., *Targeting redox heterogeneity to counteract drug tolerance in replicating*
725 *Mycobacterium tuberculosis.* Sci Transl Med, 2019. **11**(518).

726 15. Hatzios, S.K. and C.R. Bertozzi, *The regulation of sulfur metabolism in Mycobacterium*
727 *tuberculosis.* PLoS Pathog, 2011. **7**(7): p. e1002036.

728 16. Foglino, M., et al., *A direct sulfhydrylation pathway is used for methionine biosynthesis in*
729 *Pseudomonas aeruginosa.* Microbiology (Reading), 1995. **141 (Pt 2)**: p. 431-9.

730 17. Belfaiza, J., et al., *Direct sulfhydrylation for methionine biosynthesis in Leptospira meyeri.* J
731 Bacteriol, 1998. **180**(2): p. 250-5.

732 18. Hwang, B.J., et al., *Corynebacterium glutamicum utilizes both transsulfuration and direct*
733 *sulfhydrylation pathways for methionine biosynthesis.* J Bacteriol, 2002. **184**(5): p. 1277-86.

734 19. Griffin, J.E., et al., *High-resolution phenotypic profiling defines genes essential for*
735 *mycobacterial growth and cholesterol catabolism.* PLoS Pathog, 2011. **7**(9): p. e1002251.

736 20. Murphy, K.C., K. Papavinasasundaram, and C.M. Sassetti, *Mycobacterial recombineering.*
737 Methods Mol Biol, 2015. **1285**: p. 177-99.

738 21. Griffin, J.E., et al., *Cholesterol catabolism by Mycobacterium tuberculosis requires*
739 *transcriptional and metabolic adaptations.* Chem Biol, 2012. **19**(2): p. 218-27.

740 22. Chang, J.C., et al., *igr Genes and Mycobacterium tuberculosis cholesterol metabolism.* J
741 Bacteriol, 2009. **191**(16): p. 5232-9.

742 23. Srivastava, M., et al., *Molecular dynamics simulation reveals the possible druggable hot-spots*
743 *of USP7.* Oncotarget, 2018. **9**(76): p. 34289-34305.

744 24. Mittal, L., et al., *Targeting cryptic-orthosteric site of PD-L1 for inhibitor identification using*
745 *structure-guided approach.* Arch Biochem Biophys, 2021. **713**: p. 109059.

746 25. Kumari, A., et al., *Deciphering the Structural Determinants Critical in Attaining the FXR*
747 *Partial Agonism.* J Phys Chem B, 2023. **127**(2): p. 465-485.

748 26. Howe, M.D., et al., *Methionine Antagonizes para-Aminosalicylic Acid Activity via Affecting*
749 *Folate Precursor Biosynthesis in Mycobacterium tuberculosis.* Front Cell Infect Microbiol,
750 2018. **8**: p. 399.

751 27. Khan, M.Z., et al., *Redox homeostasis in Mycobacterium tuberculosis is modulated by a novel*
752 *actinomycete-specific transcription factor.* EMBO J, 2021. **40**(14): p. e106111.

753 28. Gouzy, A., et al., *Growth of Mycobacterium tuberculosis at acidic pH depends on lipid*
754 *assimilation and is accompanied by reduced GAPDH activity.* Proc Natl Acad Sci U S A, 2021.
755 **118**(32).

756 29. Loewen, P.C., *Levels of glutathione in Escherichia coli.* Can J Biochem, 1979. **57**(2): p. 107-
757 11.

758 30. Akhova, A.V. and A.G. Tkachenko, *ATP/ADP alteration as a sign of the oxidative stress*
759 *development in Escherichia coli cells under antibiotic treatment.* FEMS Microbiol Lett, 2014.
760 **353**(1): p. 69-76.

761 31. Singh, S., et al., *Unraveling the role of the transcriptional regulator VirS in low pH-induced*
762 *responses of Mycobacterium tuberculosis and identification of VirS inhibitors.* J Biol Chem,
763 2019. **294**(26): p. 10055-10075.

764 32. Mehta, M., R.S. Rajmani, and A. Singh, *Mycobacterium tuberculosis WhiB3 Responds to*
765 *Vacuolar pH-induced Changes in Mycothiol Redox Potential to Modulate Phagosomal*
766 *Maturation and Virulence.* J Biol Chem, 2016. **291**(6): p. 2888-903.

767 33. Banerjee, S.K., et al., *The sensor kinase MtrB of Mycobacterium tuberculosis regulates hypoxic*
768 *survival and establishment of infection.* J Biol Chem, 2019. **294**(52): p. 19862-19876.

769 34. Choudhary, E., et al., *Deciphering the Proteomic Landscape of Mycobacterium tuberculosis in*
770 *Response to Acid and Oxidative Stresses.* ACS Omega, 2022. **7**(30): p. 26749-26766.

771 35. Rohde, K.H., et al., *Linking the transcriptional profiles and the physiological states of*
772 *Mycobacterium tuberculosis during an extended intracellular infection.* PLoS Pathog, 2012.
773 **8**(6): p. e1002769.

774 36. Saini, V., et al., *Hydrogen sulfide stimulates Mycobacterium tuberculosis respiration, growth*
775 *and pathogenesis.* Nat Commun, 2020. **11**(1): p. 557.

776 37. Kunota, T.T.R., et al., *Mycobacterium tuberculosis H2S Functions as a Sink to Modulate*
777 *Central Metabolism, Bioenergetics, and Drug Susceptibility.* Antioxidants (Basel), 2021. **10**(8).

778 38. Rahman, M.A., et al., *The Role of Host-Generated H2S in Microbial Pathogenesis: New*
779 *Perspectives on Tuberculosis.* Front Cell Infect Microbiol, 2020. **10**: p. 586923.

780 39. Rahman, M.A., et al., *Hydrogen sulfide dysregulates the immune response by suppressing*
781 *central carbon metabolism to promote tuberculosis.* Proc Natl Acad Sci U S A, 2020. **117**(12):
782 p. 6663-6674.

783 40. Brauner, A., et al., *Distinguishing between resistance, tolerance and persistence to antibiotic*
784 *treatment.* Nat Rev Microbiol, 2016. **14**(5): p. 320-30.

785 41. Quinonez, C.G., et al., *The Role of Fatty Acid Metabolism in Drug Tolerance of Mycobacterium*
786 *tuberculosis.* mBio, 2022. **13**(1): p. e0355921.

787 42. Wu, J., et al., *Derivatives of Natural Product Agrimophol as Disruptors of Intrabacterial pH*
788 *Homeostasis in Mycobacterium tuberculosis.* ACS Infect Dis, 2019. **5**(7): p. 1087-1104.

789 43. Andreu, N., et al., *Optimisation of bioluminescent reporters for use with mycobacteria.* PLoS
790 One, 2010. **5**(5): p. e10777.

791 44. Babunovic, G.H., et al., *CRISPR Interference Reveals That All-Trans-Retinoic Acid Promotes*
792 *Macrophage Control of Mycobacterium tuberculosis by Limiting Bacterial Access to*
793 *Cholesterol and Propionyl Coenzyme A.* mBio, 2022: p. e0368321.

794 45. Pandey, A.K. and C.M. Sassetti, *Mycobacterial persistence requires the utilization of host*
795 *cholesterol.* Proc Natl Acad Sci U S A, 2008. **105**(11): p. 4376-80.

796 46. Schmittgen, T.D. and K.J. Livak, *Analyzing real-time PCR data by the comparative C(T)*
797 *method.* Nat Protoc, 2008. **3**(6): p. 1101-8.

798 47. Vocat, A., et al., *Bioluminescence for assessing drug potency against nonreplicating*
799 *Mycobacterium tuberculosis.* Antimicrob Agents Chemother, 2015. **59**(7): p. 4012-9.

800 48. Bhaskar, A., et al., *Reengineering redox sensitive GFP to measure mycothiol redox potential*
801 *of Mycobacterium tuberculosis during infection.* PLoS Pathog, 2014. **10**(1): p. e1003902.

802 49. Folch, J., M. Lees, and G.H. Sloane Stanley, *A simple method for the isolation and purification*
803 *of total lipides from animal tissues.* J Biol Chem, 1957. **226**(1): p. 497-509.

804 50. Nambi, S., et al., *The Oxidative Stress Network of Mycobacterium tuberculosis Reveals*
805 *Coordination between Radical Detoxification Systems.* Cell Host Microbe, 2015. **17**(6): p. 829-
806 37.

807 51. Mishra, R., et al., *Heterogeneous Host-Pathogen Encounters Coordinate Antibiotic Resilience*
808 *in Mycobacterium tuberculosis.* Trends Microbiol, 2021. **29**(7): p. 606-620.

809 52. Cai, Y., et al., *Host immunity increases Mycobacterium tuberculosis reliance on cytochrome*
810 *bd oxidase.* PLoS Pathog, 2021. **17**(7): p. e1008911.

811 53. Tripathi, A., et al., *Mycobacterium tuberculosis requires SufT for Fe-S cluster maturation,*
812 *metabolism, and survival in vivo.* PLoS Pathog, 2022. **18**(4): p. e1010475.

813 54. Huerta-Cepas, J., et al., *eggNOG 5.0: a hierarchical, functionally and phylogenetically*
814 *annotated orthology resource based on 5090 organisms and 2502 viruses.* Nucleic Acids Res,
815 2019. **47**(D1): p. D309-D314.

816 55. Thompson, J.D., D.G. Higgins, and T.J. Gibson, *CLUSTAL W: improving the sensitivity of*
817 *progressive multiple sequence alignment through sequence weighting, position-specific gap*
818 *penalties and weight matrix choice.* Nucleic Acids Res, 1994. **22**(22): p. 4673-80.

819 56. Berman, H.M., et al., *The Protein Data Bank.* Nucleic Acids Res, 2000. **28**(1): p. 235-42.

820 57. Baugh, L., et al., *Increasing the structural coverage of tuberculosis drug targets.* Tuberculosis
821 (Edinb), 2015. **95**(2): p. 142-8.

822 58. Sastry, G.M., et al., *Protein and ligand preparation: parameters, protocols, and influence on*
823 *virtual screening enrichments.* J Comput Aided Mol Des, 2013. **27**(3): p. 221-34.

824 59. Morris, G.M., et al., *AutoDock4 and AutoDockTools4: Automated docking with selective*
825 *receptor flexibility.* J Comput Chem, 2009. **30**(16): p. 2785-91.

826 60. Jacobson, M.P., et al., *A hierarchical approach to all-atom protein loop prediction.* Proteins,
827 2004. **55**(2): p. 351-67.

828 61. Bowers, K.J.C., E.; Xu, H.; Dror, R. O.; Eastwood, M. P.; Gregersen, B. A.; Klepeis, J. L.;
829 Kolossvary, I.; Moraes, M. A.; Sacerdoti, F. D.; Salmon, J. K.; Shan, Y.; Shaw, D. E., , *Scalable*
830 *algorithms for molecular dynamics simulations on commodity clusters.* Proceedings of the
831 ACM/IEEE Conference on Supercomputing (SC06), 2006.

832 62. Humphrey, W., A. Dalke, and K. Schulten, *VMD: visual molecular dynamics.* J Mol Graph,
833 1996. **14**(1): p. 33-8, 27-8.

834

1 **Figures and Legends.**

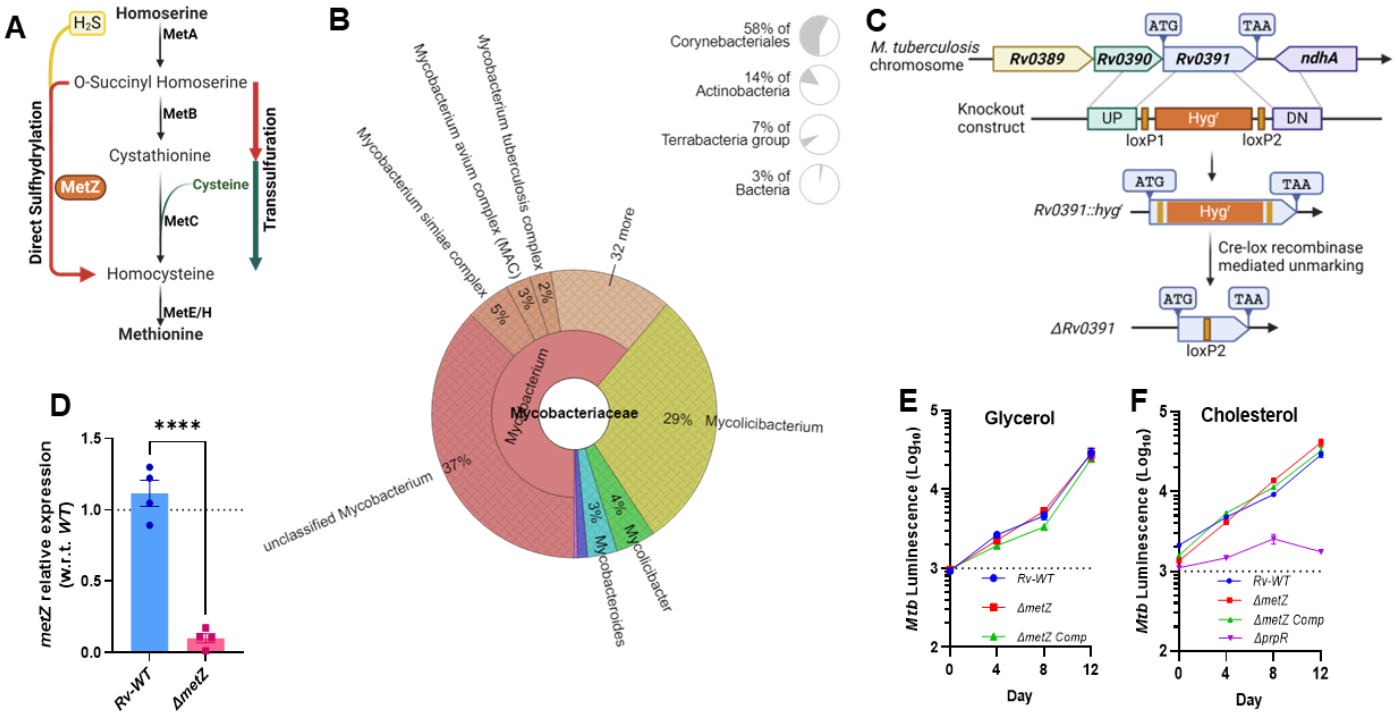

2 **Figure 1. *metZ* is dispensable for growth in *M. tuberculosis.*** (A). Methionine biosynthesis pathways in
3 bacteria. There exist two alternative pathways in many bacterial species – transsulfuration where cysteine
4 is used as sulfur-donor (S-donor) and direct sulfhydrylation where in H_2S is used as S-donor. *Rv0391*
5 encoded MetZ is such putative O-succinylhomoserine sulfhydrylase (OSHS) involved in direct
6 sulfhydrylation in *M. tuberculosis*. (B). Cluster of orthologues analysis for *M. tuberculosis* MetZ (Rv0391)
7 protein sequence with member species of ENOG502GJ5S as indicated by EggNog database. (C). Schematic
8 for knockout generation of *ΔmetZ* in *M. tuberculosis.* (D). Confirmation of *metZ* knockout using RT-qPCR
9 for the loss of *metZ* transcript. Growth kinetics of auto bioluminescent *ΔmetZ* with (E) glycerol (0.1%) and
10 (F) cholesterol (150µM) as C-source. The data summary represents mean ± SEM for technical replicates
11 and is representation of two independent experiments. Statistical comparisons were made w.r.t. Rv-WT for
12 (D) using Unpaired *t*-test. ****, $P<0.0001$. Comparisons not marked with statistical significance were not
13 significant with Rv-WT vs *ΔmetZ* for (E) and (F).

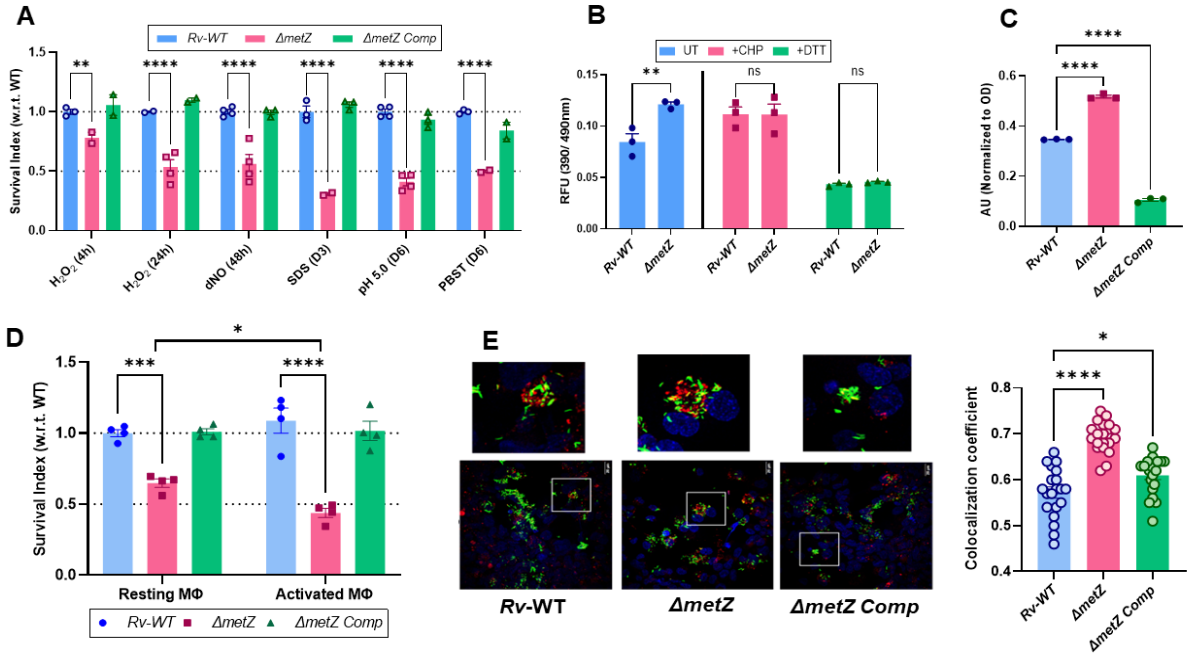

Figure 2: *metZ* deletion renders *M. tuberculosis* sensitive to physiological stressors and lead to reduced *ex-vivo* fitness. (A). *In-vitro* stress survival assay. Mycobacterial cultures were treated with reagents mimicking host-induced stresses: H_2O_2 (Oxidative stress), DetaNO (Nitrosative stress), SDS (Surfactant stress), low pH (5.0), PSBT (nutrient starvation) *in-vitro* and survival was determined by CFU plating. *ΔmetZ* was comparatively more susceptible (~40-60%) to the stressors. (B). Intra bacterial redox state determination of *ΔmetZ* as compared to Rv-WT using genetically encoded redox biosensor Mrx1-roGFP2. (C). Lipid hydroperoxidation levels in *ΔmetZ* compared to Rv-WT and complement strains using FOX2 colorimetric assay. (D). Intra-macrophage survival assay using THP-1 monocytes derived macrophages either resting or activated using IFN-γ. Survival index was determined by CFU enumeration. (E). Intracellular co-localization of GFP labeled mycobacterial strains with LysoTracker stained acidic compartments inside IFN-γ activated macrophages. Colocalization coefficient in case of *ΔmetZ* was recorded ~1.2 fold higher than Rv-WT and complement strains. The points represent replicates per group and data represented is where *ΔmetZ* is compared to Rv-WT for statistical significance. Statistics were performed using two-way ANOVA (multiple comparisons) for (A), (B), (D) and Ordinary one-way ANOVA (Dunnett's multiple comparisons test) for (C) and (E). *, P<0.05; **, P<0.01; ***P<0.001; ****P<0.0001; ns, non-significant.

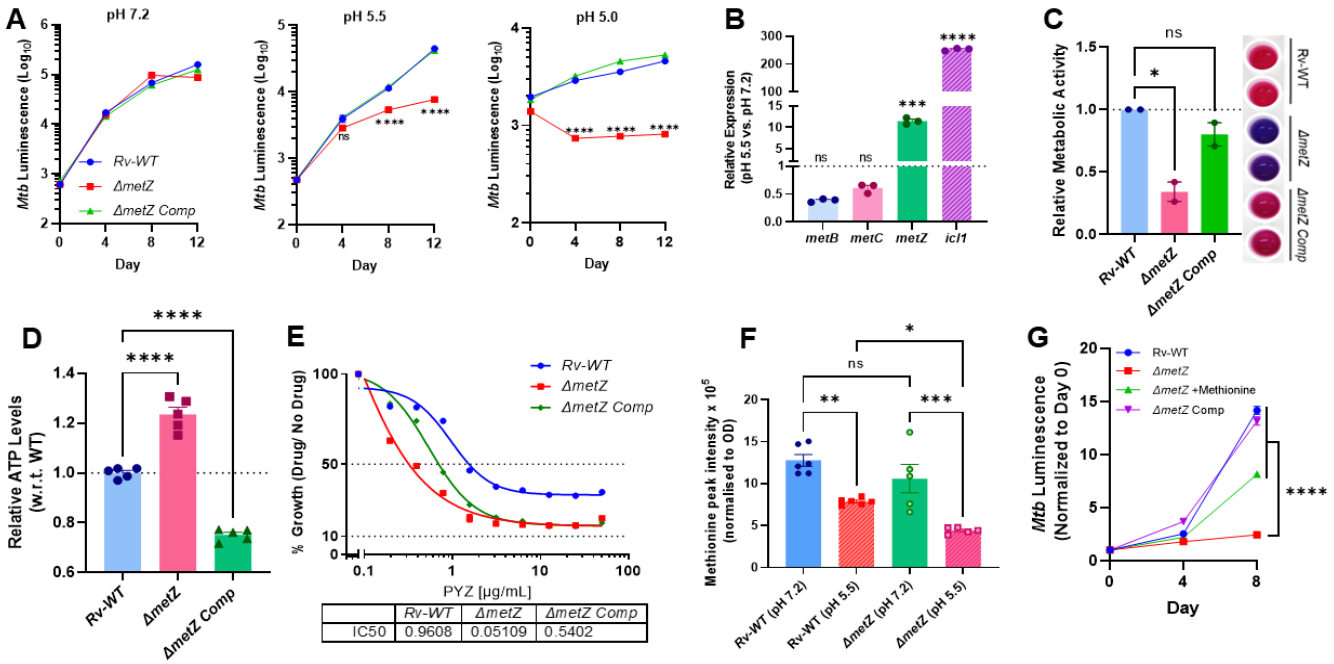

Figure 3: Direct sulfhydrylation pathway is essential for *M. tuberculosis* to survive under low pH. (A) *In-vitro* growth kinetics of *ΔmetZ* at various pH – 7.2, 5.5 and 5.0. (B). Expression analysis of genes involved in transsulfuration (*metB* and *metC*) and direct sulfhydrylation (*metZ*) using RT-qPCR. Relative expression of *metZ* was ~12-fold higher at acidic pH as compared to neutral pH. *Icl1* was used as a positive control for acidic conditions. (C). Metabolic activity of *ΔmetZ* at acidic pH using redox dye AlamarBlue Assay. (D). Intra bacterial ATP levels estimation of *ΔmetZ* at acidic pH 5.5. (E). Pyrazinamide sensitivity assay of *ΔmetZ* at pH 5.5. IC50 of PYZ for the respective strains at acidic pH 5.5 were determined and represented as dose-response curve. (F). Methionine estimation in Rv-WT and *ΔmetZ* at pH 7.2 and pH 5.5 was done using LC-MS. (G). Growth defect in *ΔmetZ* at pH 5.5 was rescued using exogenous supplementation of methionine. Dose-response curve for PYZ was made by Non-linear regression analysis using GraphPad Prism. Data is represented as the mean ± SEM of the replicates indicated by points in the respective graphs. Comparisons for statistical significance have been made with Rv-WT (except B) using two-way ANOVA (multiple comparisons) for (A) and (G); ordinary one-way ANOVA (Dunnett's Multiple Comparisons Test) for (B), (C) and (D) and ordinary one-way ANOVA (Sidak's Multiple Comparisons Test) for (F). *, P<0.01; **, P<0.002; ***P<0.005; ****P<0.0001; ns, non-significant.

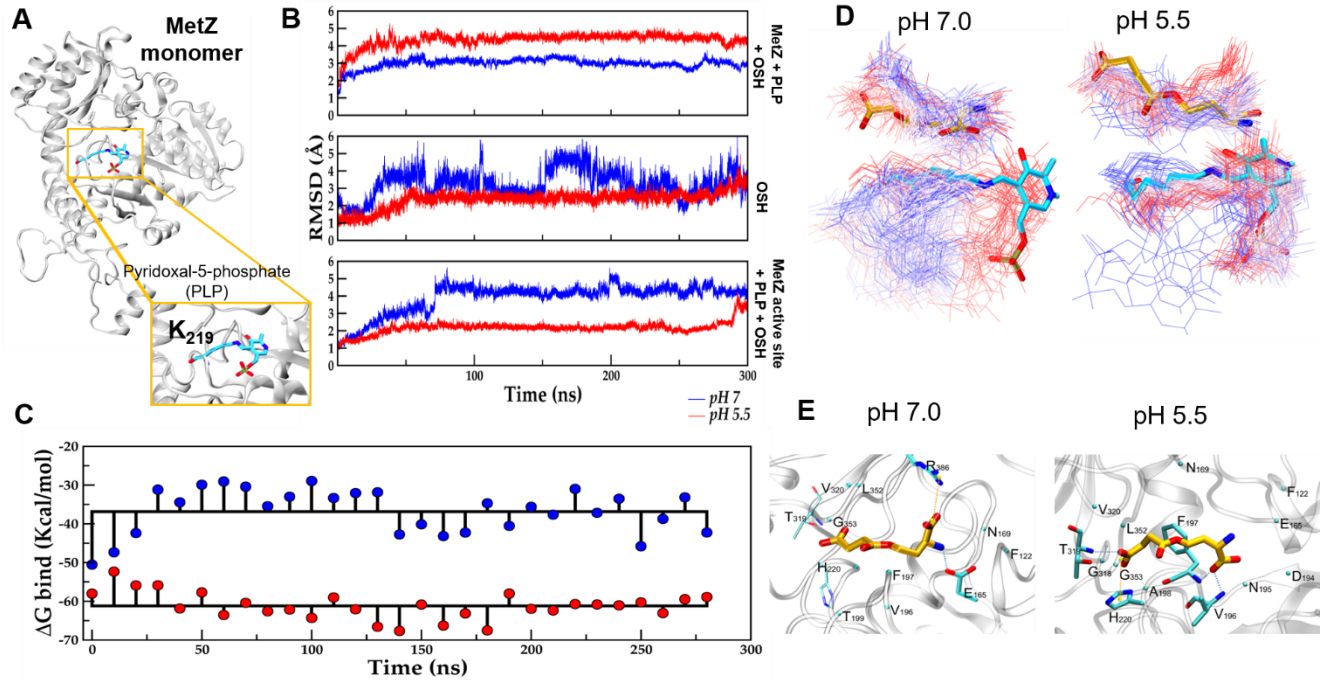

Figure 4. Molecular docking and MD simulations revealed enhanced stability of MetZ at acidic pH. (A). Structural representation of O-succinylhomoserine sulfhydrylase, rendered in new cartoon and colored in gray (single chain) with pyridoxal-5-phosphate in licorice and rendered atom-wise. (B). Dynamic characteristics of systems elucidated through constant pH MD simulations. The system's evolution is measured via RMSD through the course of 300ns of the protein, substrate and the binding site of the substrate. Color coding is followed as a system at pH 7 (blue) and at pH 5.5 (red). (C). The Binding Free Energy (in Kcal/mol) comparison of the complexes at pH 7 (blue) and pH 5.5 (red). (D). The dynamic changes represent the positional shifts of the substrate (orange) and co-factor (cyan) throughout the simulation, with a color gradient (time-dependent manner) from red (initial), white (intermediate) to blue (final) at pH 7 (a) at pH 5.5 (b). (E). Interaction map of the substrate at pH 7 and pH 5.5. Residues lining the pocket (within 4.0 Å) are shown in licorice and colored atom-wise (C: cyan, N: blue and O: red). The residues forming hydrogen bonds (dotted line in blue) and Salt-bridges (dotted line in yellow) are shown. The Cα atoms of residues involved in hydrophobic interaction are shown in beads.

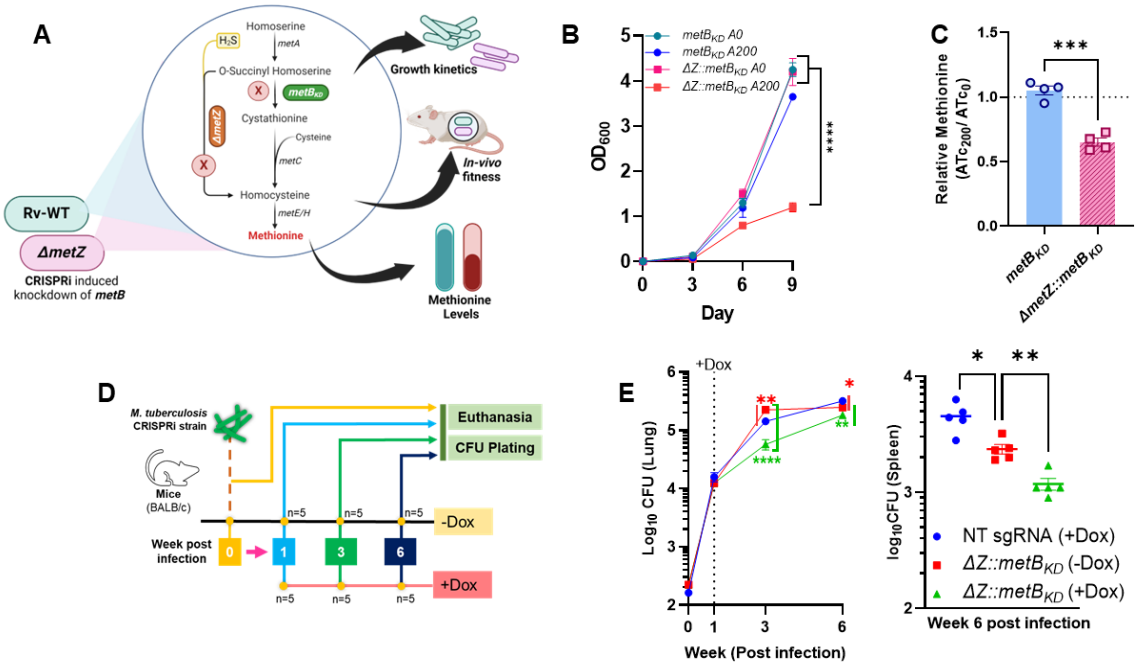

Figure 5: *metZ* mediated direct sulfhydrylation pathway is critical for methionine biosynthesis at low pH. (A). Diagrammatic representation of experimental setup to elucidate independent existence of direct sulfhydrylation pathway. CRISPRi based knockdown of *metB* (*Rv1079*) strains were generated in the genetic backgrounds of Rv-WT and *ΔmetZ* strains. These strains upon induction with ATc, were depleted of *metB* transcripts and characterized for *in-vitro* growth kinetics, methionine levels and *in-vivo* fitness. (B). *In-vitro* growth kinetics of CRISPRi knockdown strains. (C). Relative methionine levels in CRISPRi knockdown strains of *metB* and double mutant lacking both *metZ* and *metB* by LC-MS. (D). Graphical representation of *in-vivo* fitness experiment. Mice were infected with CRISPRi knockdown of *metB* in Rv-WT and *ΔmetZ* background and orally fed with doxycycline (1 mg/ml) to induce knockdown of *metB* gene in the respective strains. Bacterial burden was determined by CFU plating in lungs and spleen homogenates. (E).and (F). Bacterial burden of mycobacterial strains lacking either *metZ*, *metB* or both in mice lungs and spleen lysates respectively. Dots represent replicates per group. Statistical significance has been made using ordinary one-way ANOVA (Dunnett's Multiple Comparisons test) for (B) where ****P<0.0001; Unpaired t-test for (C) where ***P=0.0001; Mann-Whitney Test for Spleen bacterial burden in (E) where *P=0.015, **P=0.007 and two-way ANOVA (multiple comparisons) for Lungs bacterial burden in (E) where *P=0.02, **P=0.004, ***P=0.0003 and ****P<0.0001.

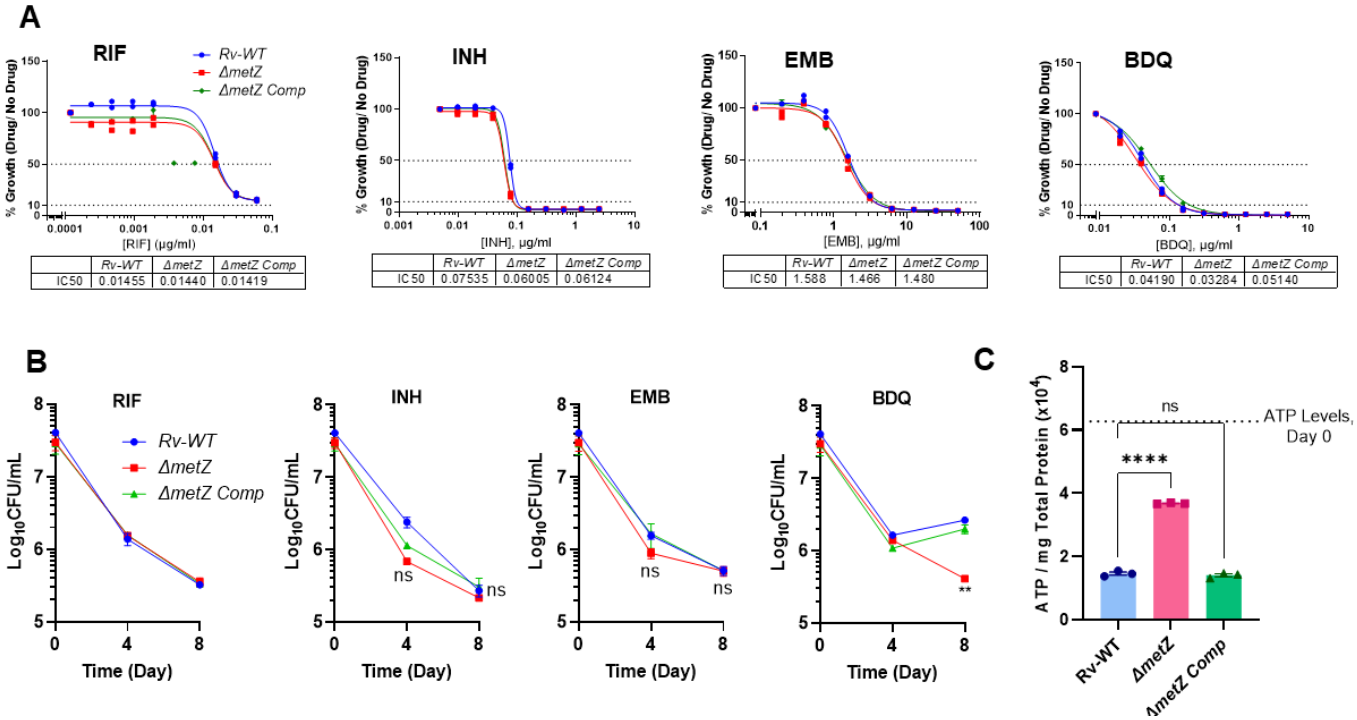

Figure 6: Direct sulfhydrylation pathway of *M. tuberculosis* contributes towards antibiotic persistence in response to Bedaquiline. (A). Minimum Inhibitory Concentration (MIC) determination of the *ΔmetZ* in comparison to Rv-WT and Complement strains against anti-TB drugs: Rifampicin (RIF), Isoniazid (INH), Ethambutol (EMB) and Bedaquiline (BDQ) using microtiter plate assay. IC50 was determined for the drugs with mentioned strains. (B). Kill kinetics of anti-TB drugs – RIF, INH, EMB and BDQ at 10X MIC concentrations. Survival was determined in the form of viable bacterial count expressed as CFU. (C). Kinetics of ATP depletion post BDQ treatment. *ΔmetZ* along with Rv-WT and Complement strains were treated with 2X concentration of BDQ and ATP was estimated at day 8 wherein *ΔmetZ* maintained high ATP levels. Data is represented as mean ± SEM and dots represent replicates per group. Comparison for statistical significance has been made using two-way ANOVA (Dunnett's Multiple Comparisons test) for (B) where **P<0.001 and ns, non-significance; ordinary one-way ANOVA (Dunnett's Multiple Comparisons test) where ****P<0.0001 and ns, non-significance.

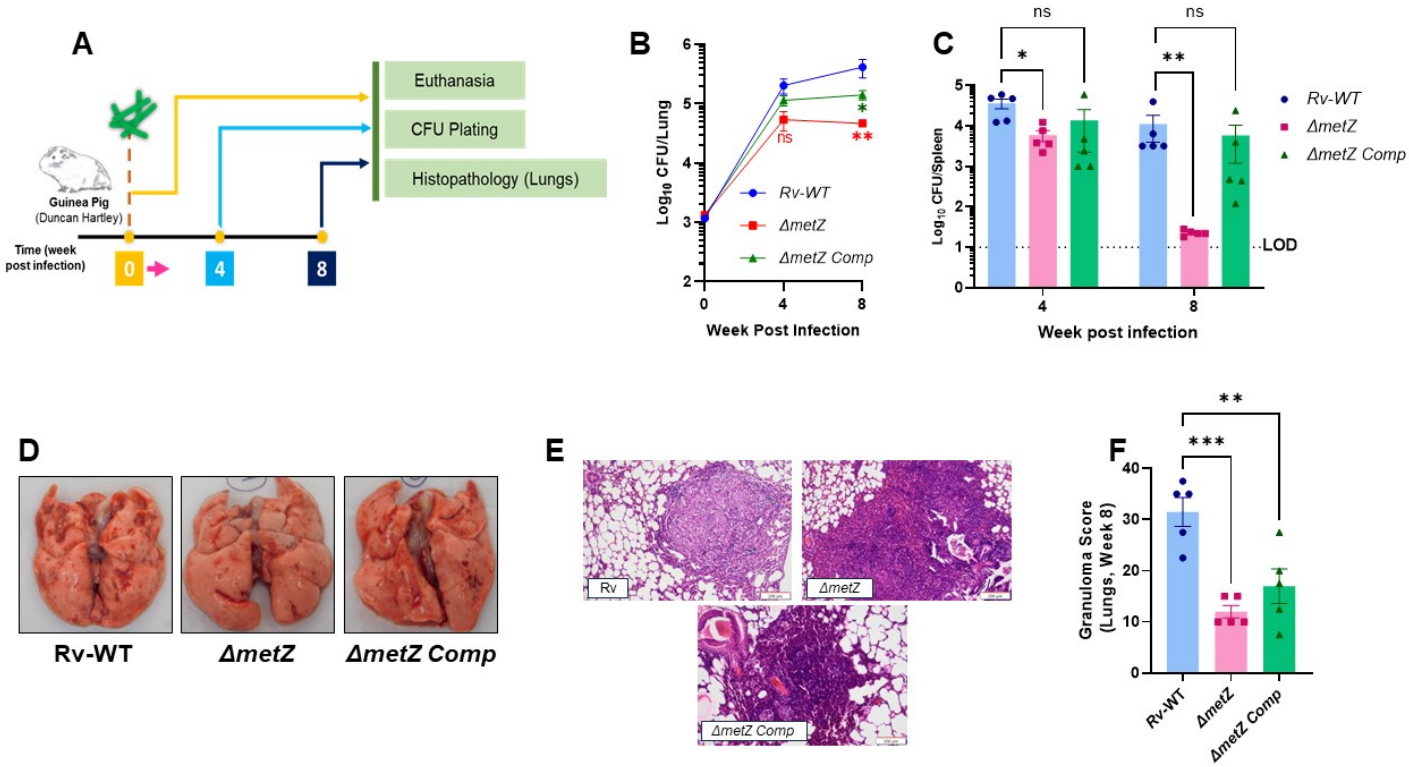

Figure 7: *metZ* is required for survival of *M. tuberculosis in-vivo*. (A). Diagrammatic representation of *in-vivo* fitness experimental set-up. Guinea pigs were infected with WT, mutant and complement strains and disease progression was monitored through CFU plating at indicated time points. (B). Bacterial burden in guinea pig lungs as determined by CFU plating of the lung homogenates of the infected animals at indicated time points. Mutant strain failed to replicate in guinea pig lungs post week 4 of initial infection. (C). CFU burden in spleens of the infected animals revealed that the mutant failed to survive inside the spleen post week 4 of infection. (D). Gross lung pathology indication lesions on the lungs at week 8 time point post aerosol infection. (E). H&E staining (F). Total granuloma scores of three strains in lung sections revealed significantly lesser granulomas in *ΔmetZ* infected lungs at week 8 post infection. Dots indicate the number of animals (or samples) per group and data is represented as mean ± SEM. Comparison for determining statistical significance has been made using Mann-Whitney Test for (B) and (C) where *P<0.05, **P=0.0079; ordinary one-way ANOVA (Dunnett's Multiple Comparisons test) where **P=0.004, ***P=0.0004.

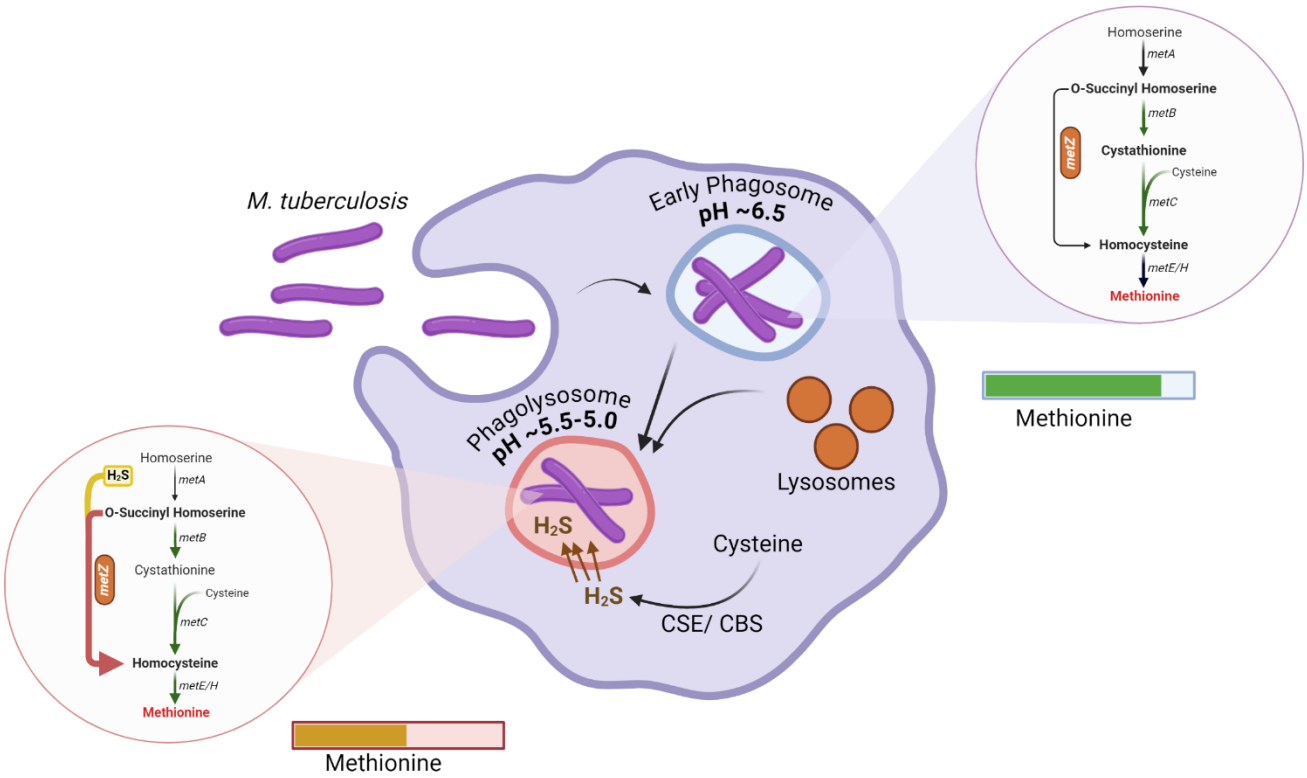

Figure 8. *metZ* driven direct sulfhydrylation is critical for methionine biosynthesis at low pH. When *M. tuberculosis* infects macrophage, it passes through a series of compartments starting from phagosome where pH is essentially ~6.5 and the bacteria is in replicating state, with enough nutrients (including methionine). Further, as host immunity kicks in and IFN-γ induces accumulation of ROS, RNS and subsequently, phagosome maturation leading to drop in pH to 5.5 and beyond, conditions are non-replicating for *M. tuberculosis* and host begins to quench nutrients from bacteria as means to impose restriction on the trapped bacteria. At this stage bacteria undergo several transcriptional and metabolic changes to sustain the host induced insults, one of these includes induction of *metZ* expression that helps bacteria survive these stress conditions and helps maintain methionine levels by utilizing endogenous as well as host generated H_2S which acts as co-substrate and S-donor for methionine biosynthesis in acidic micro-environment. This would help bacteria to maintain sufficient levels of methionine to keep adaptation going while also helps recycling of ATP, mycothiol and its metabolic activity keep going.

Supplementary Figures

pH dependent direct sulfhydrylation pathway is required for mycobacterial pathogenesis

Vaibhav Kumar Nain[1,2], Vishawjeet Barik[1,2#], Manitosh Pandey[1#], Mohit Pareek[3], Taruna Sharma[1,2], Rahul Pal[1], Shaifali Tyagi[1], Manish Bajpai[4], Prabhanjan Dwivedi[5], Bhishma Narayan Panda[5], Yashwant Kumar[4], Shailendra Asthana[3] and Amit Kumar Pandey[1,5*]

[1]Mycobacterial Pathogenesis Laboratory, Centre for Tuberculosis Research, BRIC-Translational Health Science and Technology Institute, Haryana, India

[2]Special Centre for Molecular Medicine, Jawaharlal Nehru University, New Delhi, India

[3]Computational Biophysics and CADD Group, Computational and Mathematical Biology Centre, BRIC-Translational Health Science and Technology Institute, Haryana, India

[4]Biomarker Discovery Laboratory, Non-Communicable Diseases Centre, BRIC-Translational Health Science and Technology Institute, Haryana, India

[5]Experimental Animal Facility, BRIC-Translational Health Science and Technology Institute, Haryana, India

[#] Contributed equally to this work

*** Correspondence:** Amit Kumar Pandey, amitpandey@thsti.res.in

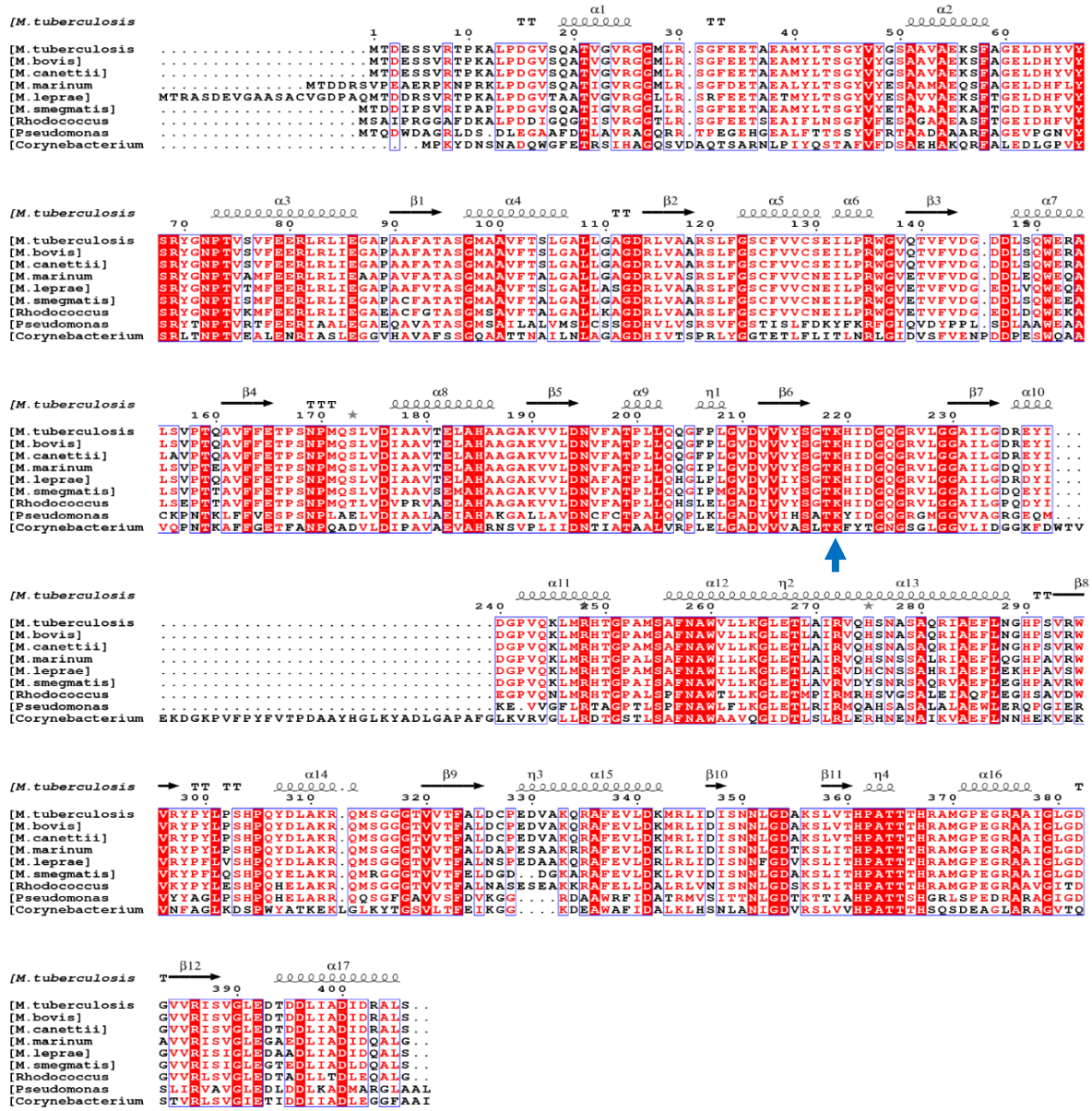

Figure S1: Rv0391 (MetZ) sequence is conserved across *Mycobacterium* genus (A). Protein sequence alignment of MetZ across other members of MTBC. Multiple sequence alignment (MSA) was done using bacterial species with gram negative (*Pseudomonas aeruginosa*) and gram-positive bacterium (*Corynebacterium glutamicum* and *Rhodococcus*) along with other mycobacterial species (*M. tuberculosis, M. bovis, M. canettii, M. marinum, M. leprae* and *M. smegmatis*). MSA revealed similarity amongst analyzed sequences wrt. Several motifs give rise to similar secondary structure (indicated by coils on top of the alignment) and conserved lysine (K219), marked by blue arrow head at which the cofactor pyridoxal-5'-phosphate is covalently attached. Presence of a characterized OSHS protein in *C. glutamicum*, in particular with similar motifs to Rv0391 indicates the probable role of MetZ (Rv0391) as an OSHS.

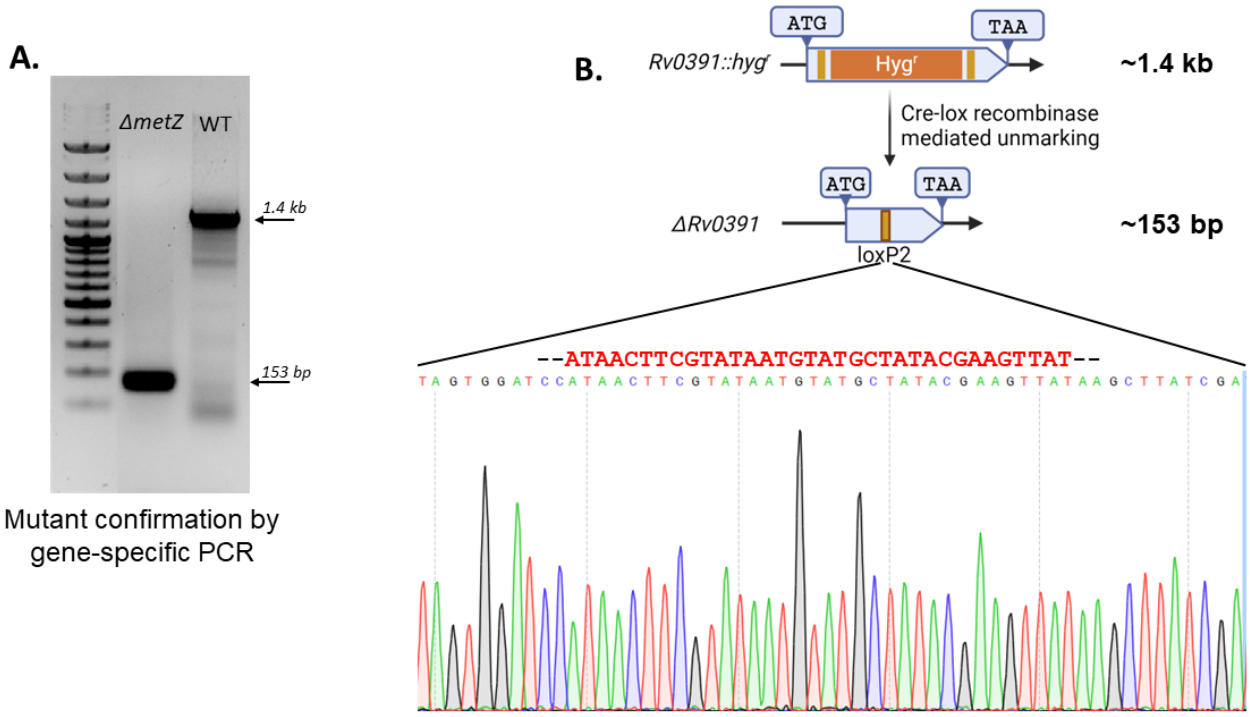

Figure S2: *Rv0391 (metZ)* genetic mutant confirmation. (A). Mutant confirmation by gene-specific PCR. Genomic DNA was isolated from the unmarked mutant culture and WT *M. tuberculosis* using which 1.4kb sized fragment encoding *metZ* gene was amplified. The unmarked mutant carried deletion of a major fragment of the said ORF thus, showing an amplicon of 153bp, confirming loss of *metZ* encoding sequence. (B). Genetic locus encoding *metZ* was sequenced in the unmarked mutant wherein, loss of the functional ORF confirmed the generation of mutant when compared to WT sequence. Post unmarking, a 34bp loxP sequence remains in the bacterial chromosome within the target sequence which serves as indicator of gene deletion and unmarking of the mutant, thereby confirming loss of Hyg^r cassette.

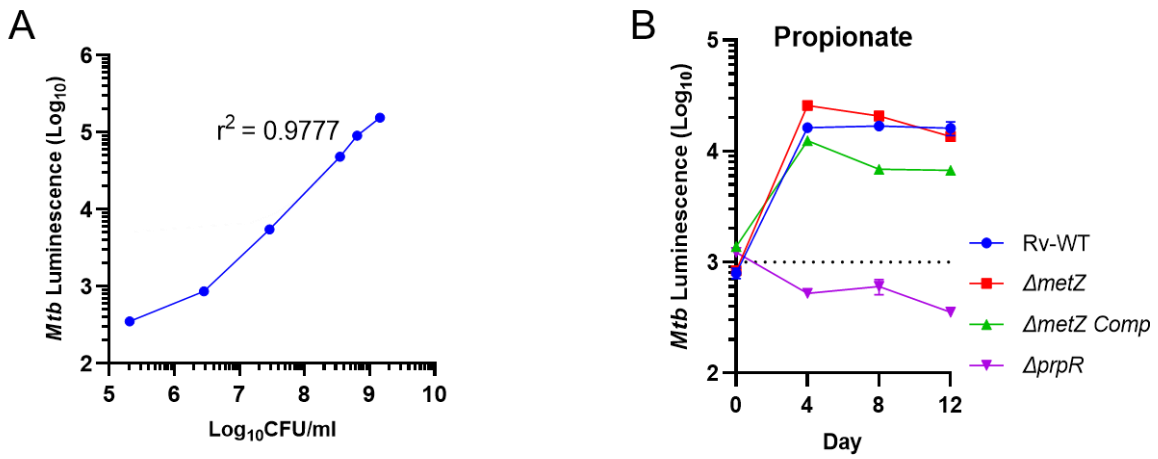

Figure S3: Generation of auto-bioluminescent Rv, *ΔmetZ* and complement stains and growth kinetics. (A). Linear regression between Luminescence and CFU in *M. tuberculosis*. Log-phase culture of *M. tuberculosis*-lux strain was grown and ~10 OD equivalent cells were serially diluted (1:10) through 0.0001. For each dilution, bacterial enumeration was done by CFU plating and luminescence was recorded. Linear relationship between luminescence and CFU was determined using linear regression analysis categorically indicating that luminescence can be used as a marker for bacterial viability and an alternative to CFU. (B) *In-vitro* growth kinetics of *ΔmetZ* in propionate (10mM) as sole C-source. Propionate is a short, odd chain fatty acid and an end product of cholesterol and fatty acid catabolism in *M. tuberculosis*.

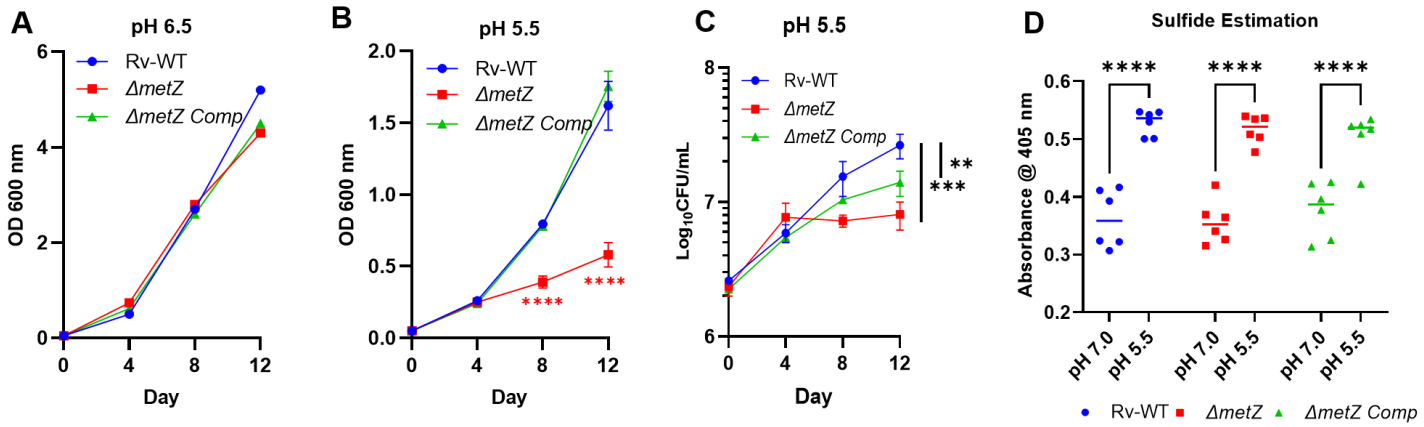

Figure S4: pH dependent growth kinetics and sulfide estimation. (A). *In-vitro* growth kinetics of *ΔmetZ* at pH 6.5. (B). *In-vitro* growth kinetics of *ΔmetZ* at pH 5.5. (C). Viable bacterial count of *ΔmetZ* in comparison to Rv-WT and Complement strains at pH 5.5 (D). Endogenous H_2S estimation in bacterial cultures of respective strains at pH 7.2 and pH 5.5 using Bismuth chloride-based colorimetric assay. Data is represented as the mean ± SEM of the replicates indicated by points in the respective graphs. Comparisons for statistical significance have been made with Rv-WT using two-way ANOVA (Dunnett's multiple comparisons test) for (B) and (C); ordinary one-way ANOVA (Sidak's Multiple Comparisons Test) for (D). **, P=0.005; ***P=0.0003; ****P<0.0001; ns, non-significant.

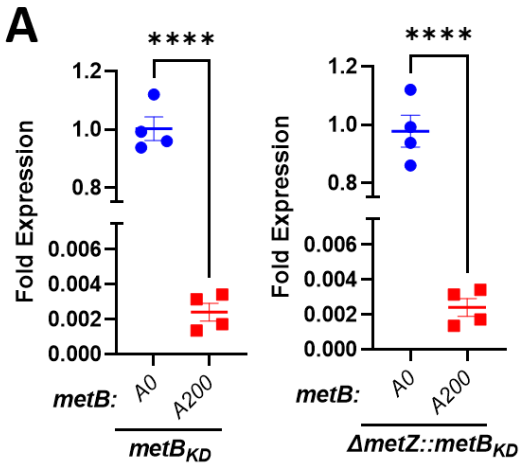

Figure S5: Confirmation of *metB$_{KD}$* using RT-qPCR. (A). CRISPRi strains were induced with ATc (200 ng/ml) and total RNA was isolated and reverse transcribed to cDNA. Further, fold expression w.r.t. ATc untreated cultures in both *Rv::metB$_{KD}$* and *ΔmetZ::metB$_{KD}$* strains were determined using the ΔΔCt method. *metB* levels were significantly reduced by several folds. Data

is represented as mean ± SEM and replicates are indicated by dots. Comparison for statistical significance has been made using Unpaired t-test where ****P<0.0001.

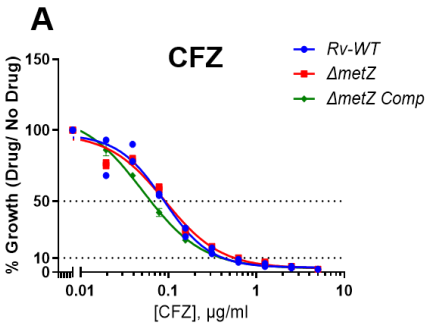

	Rv-WT	ΔmetZ	ΔmetZ Comp
IC50	0.08903	0.09110	0.05110

B MIC of anti-TB drugs

Drugs	Rv-WT	*ΔmetZ*	*ΔmetZ* Comp
	MIC_{50} (µg/ml)		
RIF	0.008	0.009	0.014
INH	0.075	0.060	0.061
BDQ	0.041	0.032	0.051
EMB	1.588	1.466	1.480
CFZ	0.089	0.091	0.051
PYZ	0.669	0.051	0.262

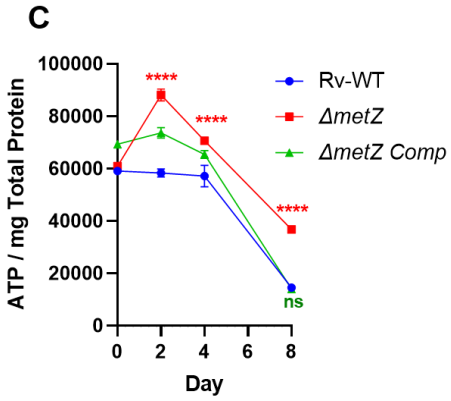

Figure S6: Drug susceptibility testing (DST) of anti-TB drugs on *Rv-WT*, *ΔmetZ* and Complement strain. (A). Dose-response curve of Clofazimine (CFZ) against the mycobacterial strains and its IC50. (B). Table summarizing IC50 values of anti-TB drugs with the respective mycobacterial strains. (C). Bedaquiline dependent ATP depletion kinetics in the indicated mycobacterial strains. Mycobacterial strains were treated with 2X BDQ for 8 days and ATP was estimated using the BacTiter-Glo kit at the indicated time-points. Data is represented as mean±SEM. Comparisons for statistical significance were made with *ΔmetZ* group using 2-way ANOVA (Dunnett's Multiple Comparisons test) where ****P, <0.0001 and ns, non-significant.

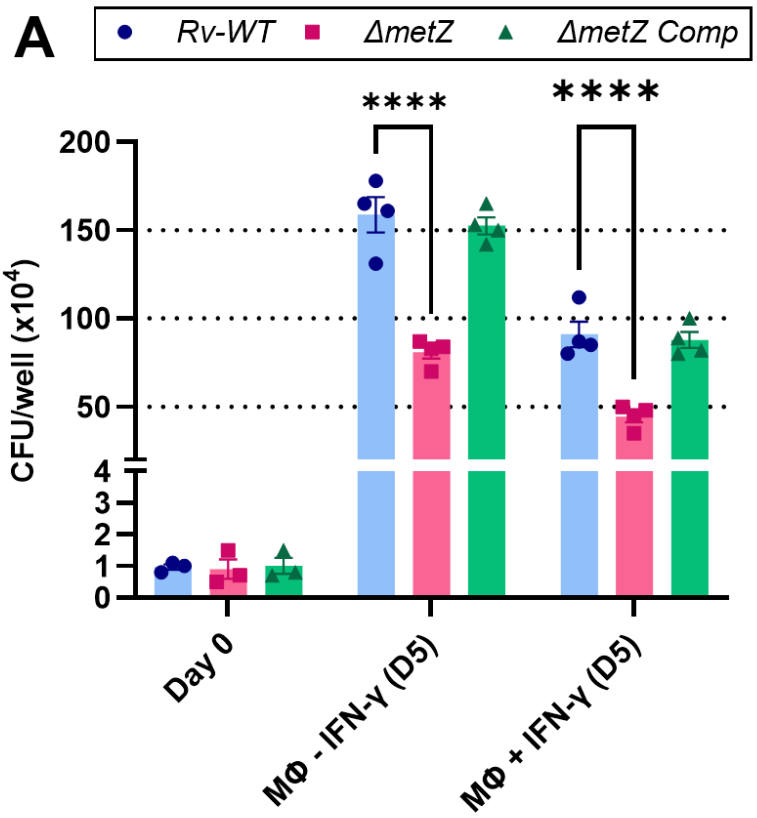

Figure S7: Intracellular survival assay. (A). Resting or IFN-g activated THP-1 macrophages were infected with Rv-WT, *ΔmetZ* and Complement strains and bacterial survival was determined by plating macrophages lysates at the indicated time-points. CFU counts show that *ΔmetZ* has compromised fitness inside resting macrophages. *ΔmetZ* CFU count is further reduced inside activated macrophages. Dots represent the replicates per group and data is shown as mean ± SEM. Comparisons have been made with Rv-WT for statistical significance using 2-way ANOVA (Dunnett's Multiple Comparisons test) where ****P <0.0001. The Survival Index calculated from the CFU values is shown in Figure 2D.

117

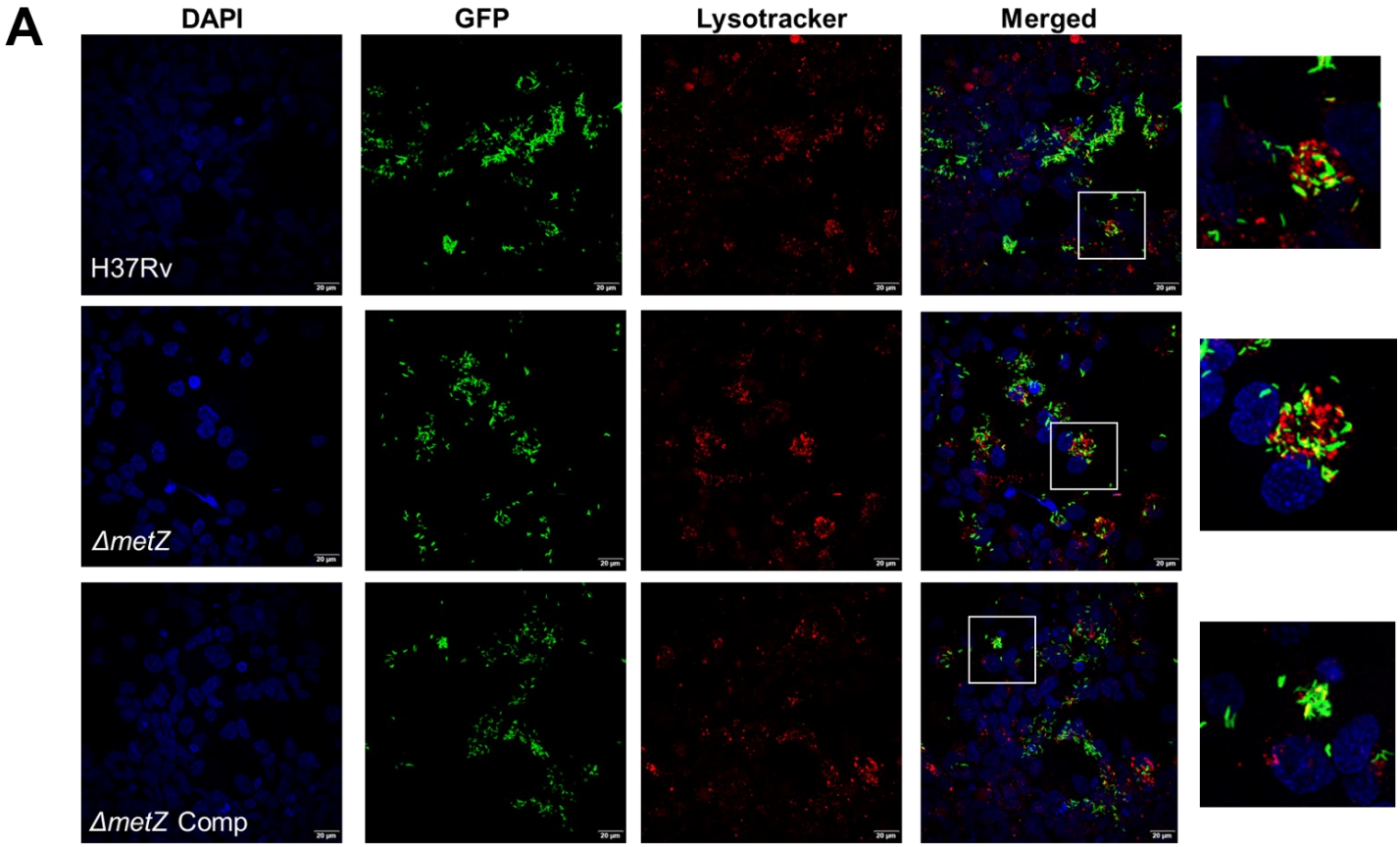

118

119 **Figure S8: Panel showing intracellular co-localization of the Rv-WT, *ΔmetZ* and Complement**
120 **strains.** mEmerald expressing mycobacterial strains were used to infect IFN-γ activated THP-1
121 macrophages. Two days after infection, the cells were fixed and stained with DAPI (for nucleus)
122 and LysoTracker Red. *ΔmetZ* cells were co-localized with acidic regions of the cells (stained in red)
123 as also indicated by higher colocalization coefficients as shown in Figure 2E. White bars indicate
124 the scale corresponding to 20μM length.

125

List of bacterial strains used in the study

S. No.	Strain	Marker	Feature	Reference
1.	*E. coli* XL1Blue			This lab
2.	*M. tuberculosis* H37Rv		Wild type *Mtb*.	Kind gift from Christopher M. Sassetti
3.	*ΔprpR::Hyg*^{r}	*Hyg*^{r}	*prpR* deletion mutant with Hyg cassette inserted in chromosomal copy of *prpR* gene (*Rv1129c*)	Kind gift from Christopher M. Sassetti
4.	*ΔprpR::Hyg*^{r}*::lux*	*Hyg*^{r}*, Kan*^{r}	*prpR* marked deletion mutant with luciferase reporter integrated at L5 attP site	This work
5.	*ΔmetZ*		*Rv0391*, *metZ* deletion mutant, umarked	This work
6.	*ΔmetZ Comp*	*Kan*^{r}	*ΔmetZ* mutant expressing pST-K:*metZ* plasmid	This work
7.	Rv::*lux*	*Zeo*^{r}*,*	Tweety int site, Luciferase reporter	This work
8.	*ΔmetZ::lux*	*Zeo*^{r}*,*	Tweety int site, Luciferase reporter	This work
9.	*ΔmetZ Comp::lux*	*Kan*^{r}*, Zeo*^{r}*,*	Tweety int site, Luciferase reporter	This work
10.	Rv: pMV261 mEmerald, TagRFP	*Hyg*^{r}*,*	Mycobacterial Live Dead Reporter expressing Rv-WT	This work
11.	*ΔmetZ*: pMV261 mEmerald, TagRFP	*Hyg*^{r}*,*	Mycobacterial Live Dead Reporter expressing *ΔmetZ* mutant	This work
12.	*ΔmetZ Comp*: pMV261 mEmerald, TagRFP	*Kan*^{r}*, Hyg*^{r}	Mycobacterial Live Dead Reporter expressing *ΔmetZ Comp* strain	This work
13.	*Rv: Mrx1-roGFP2*	*Hyg*^{r}*,*	Redox biosensor expressing Rv-WT	This work
14.	*ΔmetZ: Mrx1-roGFP21*	*Hyg*^{r}*,*	Redox biosensor expressing *ΔmetZ* mutant	This work
15.	*Rv::metB*$_{KD}$	*Kan*^{r}	WT-Mtb with *metB* gene knocked down using CRISPRi	This work
16.	*ΔmetZ::metB*$_{KD}$	*Kan*^{r}	*ΔmetZ* with *metB* gene knocked down using CRISPRi	This work
17.	*Rv::NT*$_{KD}$	*Kan*^{r}	WT-Mtb with control sgRNA (Non-targetting) CRISPRi control	This work

List of plasmids used in the study

S. No.	Plasmid	Feature	Reference
1.	pJM1	Hyg/Cm, suicidal vector for generating knockout construct for gene deletion in *M. tuberculosis*	Kind gift from Christopher M. Sassetti
2.	pST-K	Kan, episomal, mycobacterial expression vector	Kind gift from Vinay K. Nandicoori, NII, India
3.	pST-Ki	Kan, attB integrative, mycobacterial expression vector	Kind gift from Vinay K. Nandicoori, NII, India
4.	pST-K:*metZ*	Kan, pST-K backbone with metZ encoding ORF	This study
5.	pST-Ki:*metZ*	Kan, pST-Ki backbone with metZ encoding ORF	This study
6.	pMV261: mEmerald, TagRFP	Hyg, Mycobacterial Live-Dead reporter with ATc inducible RFP	Kind gift from Christopher M. Sassetti
7.	pJW276	Zeo, Integrative, Lux expressing plasmid	Kind gift from Sarah M. Fortune
8.	pMV306:LuxAB+G13	Kan, Integrative, Lux expressing plasmid	Addgene # 26161
9.	pMV762: Mrx1-roGFP2	Hyg, episomal, genetically encoded redox biosensor	Kind gift from Amit Singh, IISc, India
10.	plJR965	Kan, attB integrative, target sgRNA and $dCas9_{Sth}$ expressing plasmid for transcriptional knockdown of target gene(s) in *M. tuberculosis*	Kind gift from Sarah M. Fortune
11.	plJR965::*metB*_sgRNA	CRISPRi knockdown construct for targeting *metB* (*Rv1079*) gene in *M. tuberculosis*	This study

List of primers used in the study

S. No.	Primer Name	Sequence 5'-3'	Feature
1.	*metZ*-F1	GCTTAATTAAGTCGAGATCGAGTTTTTGGTCACC	Cloning of 1000bp upstream region of *metZ* gene for knockout construct
2.	*metZ*-R1	ATGCGGCCGCGCGGACCGAAGACTCGTC	
3.	*metZ*-F2	ATCTCGAGACCGACGACCTGATTGCCGAT	Cloning of 1000bp downstream region of *metZ* gene for knockout construct
4.	*metZ*-R2	ATCTCGAGCGGAATGAAGACCATCGACGAC	
5.	*metZ*-F	AACATATGATGACCGACGAGTCTTCGGTC	Cloning of *metZ* encoding ORF in *NdeI/ EcoRI* sites
6.	*metZ*-R	AAGAATTCTTAGCTCAACGCCCGATCGATATC	
7.	*metB*-CR-F	GGGAACCGCGCCGGCGCCGTTCTG	Cloning of *metB* targeting sgRNA
8.	*metB*-CR-R	AAACCAGAACGGCGCCGGCGCGGT	
9.	*metB*-RT-F	GGCGGCACATTCCGGTTGATA	qPCR primers of *metB*
10.	*metB*-RT-R	GTGAGGCAAAGGTATTGTCCACCA	
11.	*metC*-RT-F	GACCATCTCCAACCCGCAG	qPCR primers of *metC*
12.	*metC*-RT-R	GTCGGGGGTGGTGAAGC	
13.	*metZ*-RT-F	GACGACCTCTCGCAATGGGA	qPCR primers of *metZ*
14.	*metZ*-RT-R	GTACACCACCACGTCGACC	
15.	*sigA*-RT-F	GAAGACCACGAAGACCTCGAAG	qPCR primers of *sigA*
16.	*sigA*-RT-R	GTTTGAGGTAGGCGCGAACC	
17.	*Icl1*-RT-F		qPCR primers of *icl1*
18.	*Icl1*-RT-R		